Romanian Journal of Petroleum & Gas Technology
Vol. VII (LXXVIII) • No. 1/2026

GENETIC HOMOGENEITY AND RESERVOIR CONNECTIVITY IN THE NIGER DELTA PETROLEUM SYSTEM: EVIDENCE FROM INTEGRATED MULTIVARIATE BIOMARKER GEOCHEMISTRY

Timothy Chibuike Anyanwu [1*], Bassey Offiong Ekpo [2], Basil Ngozichukwu Anukam [3], Valentine Ezennubia [4], Francis Eromosele Adali [5]

[1] Department of Geology, Federal University of Technology, P.M.B., 1526, Owerri, Nigeria
[2] Petroleum & Environmental Geochemistry Research Group (PEGRG), Department of Pure and Industrial Chemistry, University of Calabar, Calabar, Nigeria
[3] Department of Chemistry, Federal University of Technology, P.M.B., 1526, Owerri, Nigeria
[4] Oklahoma State University, Stillwater, OK 74078, USA
[5] Department of Petroleum Engineering, Covenant University, Ota, Nigeria
* E-mail (corresponding author): tcanyanwu@futo.edu.ng

DOI: 10.51865/JPGT.2026.01.18

ABSTRACT

Reservoir connectivity remains a major source of uncertainty in structurally complex deltaic petroleum systems, where fault segmentation and stratigraphic heterogeneity may obscure fluid communication. This study evaluates basin-scale reservoir connectivity across the major depobelts of the Niger Delta Basin using integrated oil geochemical fingerprinting and multivariate statistical analysis. Twenty-five crude oil samples from producing reservoirs in the Northern Delta, Greater Ughelli, Central Swamp, Coastal Swamp, and Shallow Offshore depobelts were analyzed using gas chromatography–mass spectrometry (GC–MS). Diagnostic biomarker parameters were statistically evaluated using hierarchical cluster analysis (HCA), principal component analysis (PCA), correlation analysis, and radar plot visualization. Biomarker distributions indicate strong compositional similarity among the oils, characterized by mixed terrestrial–marine organic matter input, deltaic depositional conditions, and comparable thermal maturity. HCA results reveal tight clustering of samples at low linkage distances, with extensive intermixing of oils from different depobelts. PCA shows that 79.48% of total variance is explained by five principal components, dominated by terrestrial input and redox-sensitive biomarker ratios, while maturity-related parameters contribute secondary variability. The absence of discrete clustering in multivariate space demonstrates that the oils belong to a single dominant genetic family. The integrated geochemical and statistical evidence indicates basin-scale charge system continuity and extensive migration across structurally distinct depobelts. These findings demonstrate that structural compartmentalization in the Niger Delta does not necessarily equate to geochemical isolation.

Keywords: Reservoir connectivity, oil geochemistry, biomarkers, multivariate analysis, Niger Delta Basin.

Romanian Journal of Petroleum & Gas Technology
Vol. VII (LXXVIII) • No. 1/2026

INTRODUCTION

Reservoir connectivity is a fundamental control on hydrocarbon migration efficiency, pressure communication, production performance, and ultimate recovery in petroleum systems. In structurally complex sedimentary basins, uncertainty in reservoir connectivity remains a major source of technical and economic risk, particularly where faulting, stratigraphic heterogeneity, and shale-rich intervals introduce potential barriers to fluid flow [1],[2],[3],[4]. Accurate evaluation of connectivity is therefore essential for reserve estimation, infill drilling decisions, and long-term reservoir management. Deltaic petroleum systems are especially prone to connectivity uncertainty due to rapid lateral facies variations, syn-depositional faulting, and prolonged, multi-phase hydrocarbon charge histories. The Niger Delta Basin represents a classic example of such complexity (Figure 1). As one of the world's most prolific hydrocarbon provinces, it accounts for the majority of Nigeria's oil and gas production and hosts hundreds of producing fields distributed across a series of structurally and stratigraphically distinct depobelts [5],[6],[7]. Despite decades of exploration and production, significant uncertainty persists regarding the degree of fluid communication within and across these depobelts, largely because structural compartmentalization inferred from seismic interpretation does not always correspond to geochemical or dynamic isolation [8],[9]. The structural framework of the Niger Delta is dominated by gravity-driven deformation related to rapid sediment loading on over-pressured marine shales of the Akata Formation.

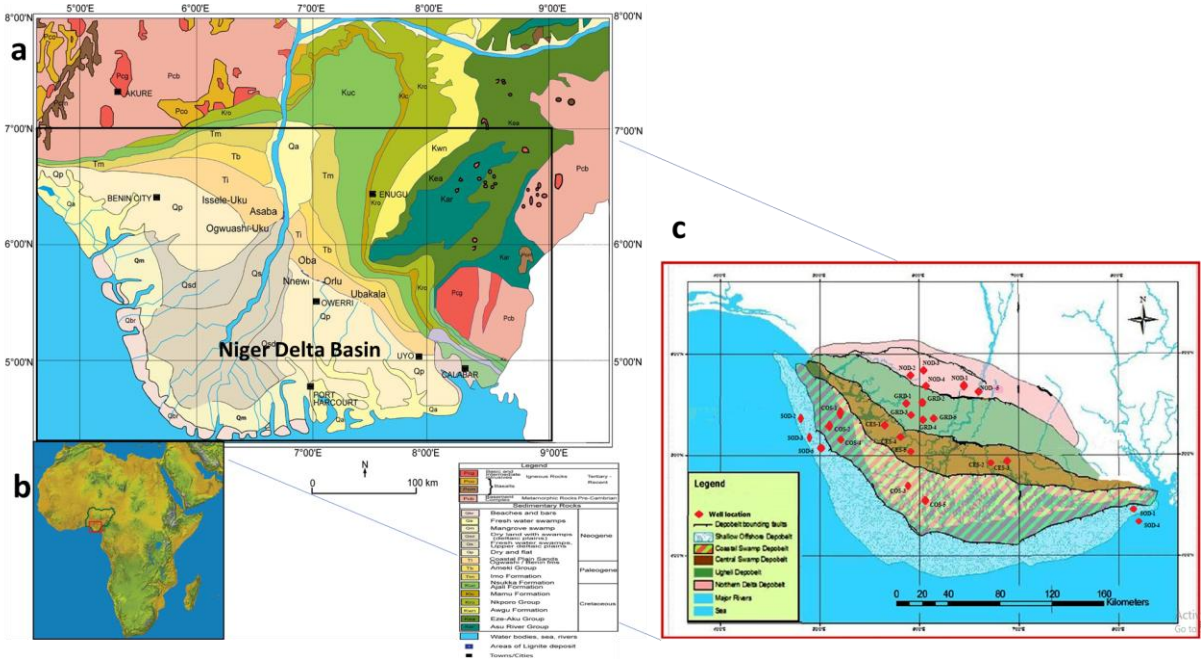

Figure 1. *Geologic map of the study area: (a) Map of the Southeastern Nigeria sedimentary basins showing the location of the Niger Delta; (b) Map of the African continent indicating the location of Nigeria;(c) Outline map of the Niger Delta. Red Stars show the locations of the twenty-five wells in the five depobelts from which crude oil samples were collected for this study.*

This deformation has produced extensive listric growth faults, rollover anticlines, antithetic fault systems, shale diapirs, and collapsed crest structures [5],[10]. These structures may act either as conduits that facilitate hydrocarbon migration or as effective seals that compartmentalize reservoirs, depending on fault throw, shale smear continuity, and the timing

of deformation relative to hydrocarbon generation and migration [6]. Consequently, reservoirs that appear structurally isolated may be geochemically connected, while reservoirs that appear structurally linked may behave as independent compartments during production.

Conventional approaches to reservoir connectivity assessment such as pressure transient analysis, production data interpretation, and seismic fault seal analysis are often limited by data availability, scale dependency, and interpretational ambiguity, particularly in mature or data-restricted fields. These methods primarily reflect present day or production-time behavior and may not capture the integrated geological history of hydrocarbon charge and migration. As a result, geochemical techniques have increasingly been adopted as complementary tools for evaluating reservoir connectivity because they preserve information accumulated over geological time scales [2],[11]. Oil geochemical fingerprinting is based on the principle that crude oil composition reflects its source organic matter, depositional environment, thermal maturity, migration pathway, and post-accumulation alteration history. Oils generated from the same source rock and charged through connected migration pathways typically display closely similar molecular compositions, whereas significant compositional differences may indicate compartmentalization, multiple charge events, biodegradation, or mixing from different sources [3],[9],[12]. Whole-oil gas chromatography and biomarker analysis focusing on n-alkanes, isoprenoids, steranes, hopanes, and oleanane have therefore become widely used tools for oil–oil correlation and reservoir connectivity assessment.

In the Niger Delta, numerous studies have demonstrated the effectiveness of oil geochemistry for petroleum system characterization. Biomarker evidence consistently indicates that most Niger Delta oils are derived from mixed terrestrial - marine organic matter deposited in deltaic to shallow-marine environments and generated primarily from Paleogene source rocks, particularly the Akata Formation [13],[14],[15],[16],[17]. More recent studies integrating biomarker data with multivariate statistical techniques have suggested that crude oils from different fields and depobelts commonly belong to a single dominant genetic oil family, implying extensive lateral and vertical migration and basin-scale mixing [9],[4]. Multivariate statistical methods, especially hierarchical cluster analysis (HCA), provide an objective framework for evaluating similarities and differences among large geochemical datasets. When combined with graphical visualization tools such as star (radar) plots, these methods allow multiple independent geochemical parameters to be assessed simultaneously, enhancing the robustness of reservoir connectivity interpretations [2]. This integrated approach is particularly valuable in structurally complex deltaic basins, where simple one-parameter correlations may be misleading. Despite the growing body of geochemical work in the Niger Delta, basin-scale evaluations of reservoir connectivity that explicitly integrate biomarker geochemistry with multivariate statistical analysis across multiple depobelts remain limited. Given the continued importance of field redevelopment, enhanced recovery, and exploration risk reduction in the basin, a comprehensive assessment of oil connectivity at the depobelt scale is both timely and necessary. This study addresses this gap by applying an integrated oil geochemical and multivariate statistical approach to evaluate reservoir connectivity across the major depobelts of the Niger Delta Basin. Twenty-five crude oil samples from producing reservoirs in the Northern Delta, Greater Ughelli, Central Swamp, Coastal Swamp, and Shallow Offshore depobelts were analyzed using whole-oil gas chromatography and gas chromatography–mass spectrometry (GC–MS). Diagnostic biomarker parameters were combined with hierarchical cluster analysis and star plot visualization to assess oil family relationships, source inputs, thermal maturity, and the extent of fluid communication within and across structurally distinct

depobelts. The objectives of this study are to: (i) characterize the molecular and biomarker fingerprints of Niger Delta crude oils; (ii) evaluate genetic relationships, source organic matter inputs, depositional conditions, and thermal maturity; and (iii) assess reservoir connectivity and charge system continuity using integrated geochemical and statistical techniques. By extending oil geochemical fingerprinting to a basin-scale framework, this study provides new insights into the dominance of petroleum system continuity over structural compartmentalization in the Niger Delta.

GEOLOGICAL SETTING

The Niger Delta Basin is a large, wave-dominated clastic delta developed along the passive continental margin of the Gulf of Guinea, West Africa. Basin evolution commenced in the Late Jurassic to Early Cretaceous following the rifting and subsequent separation of the African and South American plates, which led to the opening of the South Atlantic Ocean [6],[14],[18],[19]. From the Paleogene onward, rapid sediment supply from the Niger–Benue drainage system resulted in the progradation of a thick deltaic wedge exceeding 10 km in places. The basin fill is classically subdivided into three diachronous lithostratigraphic units (Figure 2): the Akata, Agbada, and Benin formations [5],[10],[20].

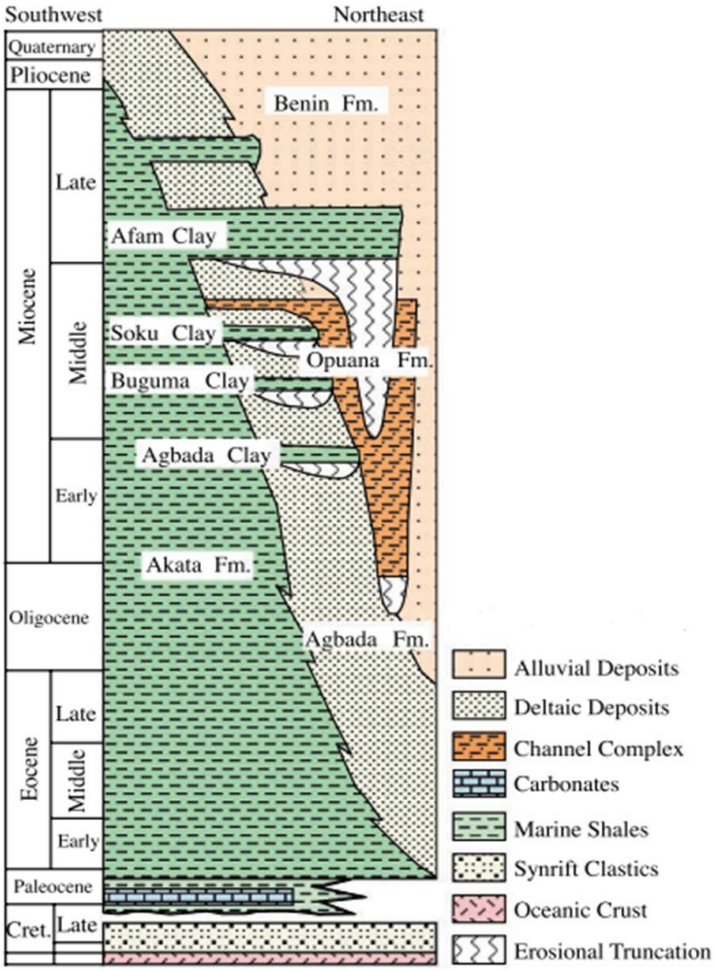

***Figure 2**. Generalized stratigraphic column of the Niger Delta Basin showing Akata, Agbada, and Benin formations* [10].

Romanian Journal of Petroleum & Gas Technology
Vol. VII (LXXVIII) • No. 1/2026

The basal Akata Formation consists predominantly of over-pressured marine shales with minor turbiditic sandstones and forms the principal source rock in the basin. The overlying Agbada Formation comprises alternating sandstone and shale units deposited in delta-front to shallow-marine environments and hosts most of the basin's hydrocarbon reservoirs [21],[22]. The Benin Formation caps the succession and is composed mainly of continental fluvial sands with negligible hydrocarbon potential. Structurally, the Niger Delta is dominated by gravity-driven extensional and compressional deformation linked to shale mobility within the Akata Formation. Rapid sediment loading triggered basinward gravitational collapse, producing large-scale listric growth faults, rollover anticlines, antithetic faults, shale diapirs, and toe-thrust structures [5],[10]. These structures are organized into a series of arcuate depobelts that young seaward and reflect successive phases of delta progradation. Each depobelt is characterized by a distinctive structural style and stratigraphic architecture, which exert first-order controls on hydrocarbon migration pathways and reservoir compartmentalization [6],[23]. While growth faults may act as migration conduits during active deformation, fault sealing due to shale smear and clay gouge development can later isolate reservoirs during production. This dual behavior complicates connectivity predictions based solely on structural interpretation. Figure 3 is a schematic structural element and depobelt framework of the Niger Delta Basin.

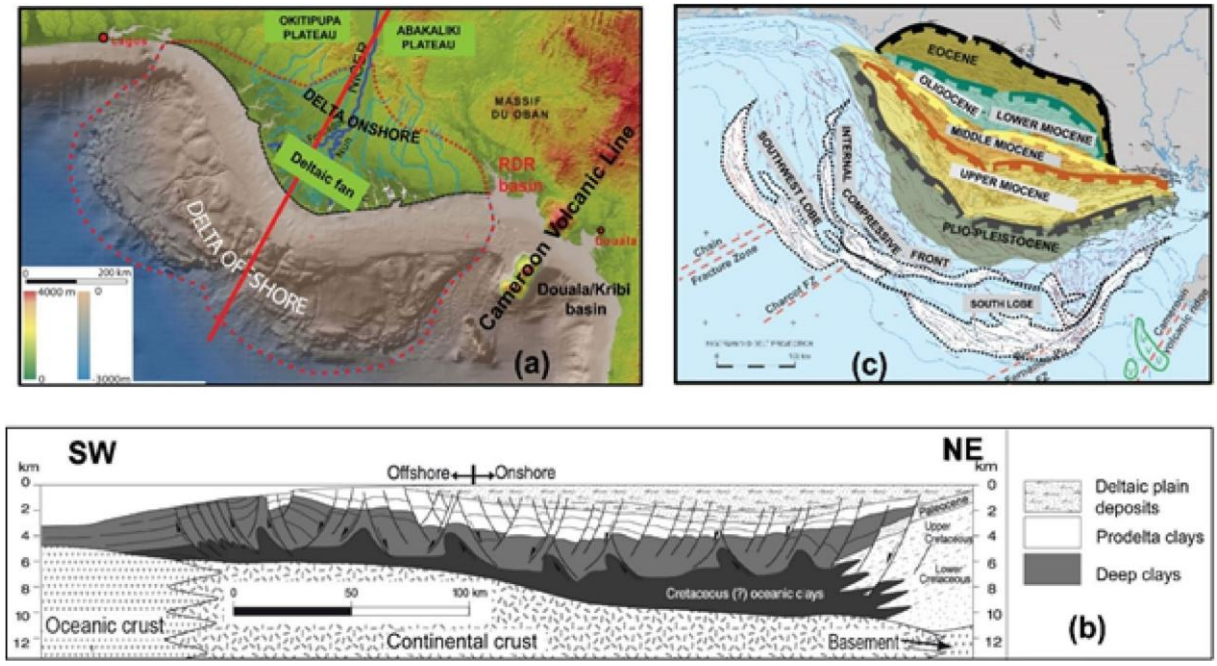

Figure 3. *Structural framework and depobelt architecture of the Niger Delta Basin: (a) Map illustrating the morphology and geographic setting of the Niger Delta; the red line indicates the location of the cross-section shown in (b); (b) NE–SW structural cross-section displaying the basin architecture, characterized by a thick sedimentary succession affected by gravity-driven deformation along one or more detachment surfaces* [37]. *The section shows an updip extensional domain balanced by a downdip compressional domain; (c) Structural map depicting the progressive and synchronous seaward migration of depobelts accompanied by widespread deformation* [24].

The Niger Delta petroleum system is dominated by hydrocarbons generated from organic-rich shales of the Akata Formation, with minor contributions from interbedded shales within the Agbada Formation [13],[14]. Source rocks are characterized by mixed terrestrial and marine

organic matter deposited under deltaic to shallow-marine conditions and have attained maturity primarily in the deeper offshore and distal onshore settings. Hydrocarbon migration occurs predominantly through fault-assisted vertical pathways and laterally through permeable sand bodies within the Agbada Formation. Multiple phases of generation and migration, coupled with continued structural deformation, have resulted in widespread charge mixing and redistribution across stratigraphic levels and depobelts [14]. Therefore, reservoirs located in different structural compartments or depobelts may be charged by genetically similar oils, even where present-day pressure communication is limited. The combination of syn-depositional faulting, shale mobility, and prolonged hydrocarbon charge history has produced a petroleum system in which structural compartmentalization does not necessarily equate to geochemical isolation.

MATERIALS AND METHODS

Sample Collection and Study Coverage

A total of twenty-five (25) crude oil samples were collected from producing reservoirs across the major depobelts of the Niger Delta Basin, including the Northern Delta, Greater Ughelli, Central Swamp, Coastal Swamp, and Shallow Offshore depobelts (Figure 1). The samples were obtained directly from wellheads or production separators to minimize contamination and alteration during handling. All samples were stored in pre-cleaned, airtight glass containers and preserved under dark, cool conditions prior to laboratory analysis.

Fractionation

Crude oil samples were subjected to column chromatography for the separation of hydrocarbon and polar fractions. The samples were loaded onto columns packed with activated silica gel (preheated at 120 °C to remove moisture) and preconditioned with petroleum ether. Sequential elution was performed using solvents of increasing polarity. The aliphatic (saturate) hydrocarbons were first eluted with 70 mL of petroleum ether, followed by the aromatic fraction using 70 mL of dichloromethane (DCM). The resin fraction, comprising more polar components, was subsequently eluted using a mixture of DCM and methanol. Each collected fraction was concentrated by solvent evaporation in a sand bath and further dried under a gentle stream of nitrogen to remove residual solvent without thermal degradation. The saturate fraction was re-dissolved in petroleum ether to a known volume for GC–MS analysis, while the aromatic and resin fractions were stored for potential further analysis.

Gas chromatography–mass spectrometry (GC–MS) Analysis

Molecular characterization of the aliphatic (saturate) fraction was performed using gas chromatography–mass spectrometry (GC–MS). Analyses were conducted on a Hewlett–Packard 5890 II gas chromatograph coupled to a mass spectrometer operating in electron impact (EI) mode at 70 eV, with the ion source maintained at 160 °C. Data were acquired in both full scan and selected ion monitoring (SIM) modes using the HP Vectra PC ChemStation software. A 1 µL aliquot of the saturate fraction was injected via an autosampler at an injector temperature of 290 °C. Separation was achieved on a DB-5 capillary column (30 m × 0.25 mm i.d., 0.25 µm film thickness) using helium as the carrier gas at a constant flow. The GC oven was programmed from 40–50 °C, ramped at 4 °C/min to 300 °C, and held isothermally for 17–20 minutes to ensure complete elution of high molecular weight compounds. Biomarkers were identified and quantified in SIM mode, monitoring m/z 191 for hopanes and m/z 217 for

steranes. Compound identification relied on mass fragmentation patterns, retention times compared with standards, literature data, and established elution order. Peak integration was performed using the instrument software, and cumulative peak areas were exported to Microsoft Excel for calculation of biomarker ratios, table preparation, and graphical representation.

Multivariate Statistical Analysis

To objectively evaluate genetic relationships, compositional variability, and reservoir connectivity among the crude oil samples, multivariate statistical analyses were applied to the selected geochemical and biomarker dataset. These analyses include hierarchical cluster analysis (HCA) and principal component analysis (PCA), which were used in a complementary manner. Prior to statistical analysis, all geochemical variables were screened for analytical consistency and standardized (z-score normalization) to eliminate bias arising from differences in units and magnitude. Only diagnostic parameters with demonstrated geochemical significance and minimal sensitivity to secondary alteration were retained.

Hierarchical Cluster Analysis (HCA)

Hierarchical cluster analysis was performed to classify the crude oil samples into genetically related groups based on overall compositional similarity. Rescaled distance was used as the similarity measure, and Ward's linkage method was applied to minimize within-cluster variance. The resulting dendrogram provides an objective framework for identifying oil families and assessing genetic relationships among samples from different reservoirs and depobelts. Samples clustering closely are interpreted to share similar source characteristics, maturity levels, and migration histories, thereby indicating potential reservoir connectivity [2].

Principal Component Analysis (PCA)

Principal component analysis (PCA) was applied to the same standardized geochemical dataset to reduce data dimensionality and to identify the principal variables controlling compositional variation among the crude oil samples. PCA transforms the original correlated variables into a smaller number of orthogonal principal components (PCs), each representing a linear combination of the original parameters and accounting for a progressively smaller proportion of the total variance in the dataset. The first few principal components, which together explain the majority of the variance, were examined to determine the dominant geochemical controls on oil composition, including source organic matter input, depositional environment, thermal maturity, and secondary alteration effects [25]. Sample scores on the principal components were used to evaluate clustering patterns and compositional overlap among oils from different reservoirs and depobelts. PCA score plots were interpreted alongside loading plots to assess which geochemical parameters exert the strongest influence on sample grouping. Oils plotting closely in PCA space are considered to be compositionally similar and likely genetically related, whereas separation along principal component axes indicates differences in source facies, maturity, or charge history. When interpreted together with HCA results, PCA provides an independent and robust means of assessing reservoir connectivity.

Star Plot Visualization

To further support the multivariate interpretations, star (radar) plots were constructed using selected biomarker ratios that showed strong discriminatory power in both HCA and PCA. Star plots allow visual comparison of multi-parameter fingerprints among representative samples within each identified oil family.

Romanian Journal of Petroleum & Gas Technology
Vol. VII (LXXVIII) • No. 1/2026

RESULTS

Molecular Characteristics

The crude oil samples display broadly similar hydrocarbon distribution patterns dominated by n-alkanes ranging from approximately n-C_{12} to n-C_{35}, with well-developed peaks in the mid- to high-molecular-weight range (Figure 4). The chromatograms generally show a smooth, unimodal distribution with minimal unresolved complex mixture (UCM), indicating limited biodegradation across the sampled reservoirs [18],[26]. The similarity of the chromatographic profiles across samples from different depobelts indicates a high degree of compositional uniformity at the bulk oil level. Most of the crude oil samples are characterized by a high proportion of saturated hydrocarbons, which supports their classification as normal (non-biodegraded) crude oils [27].

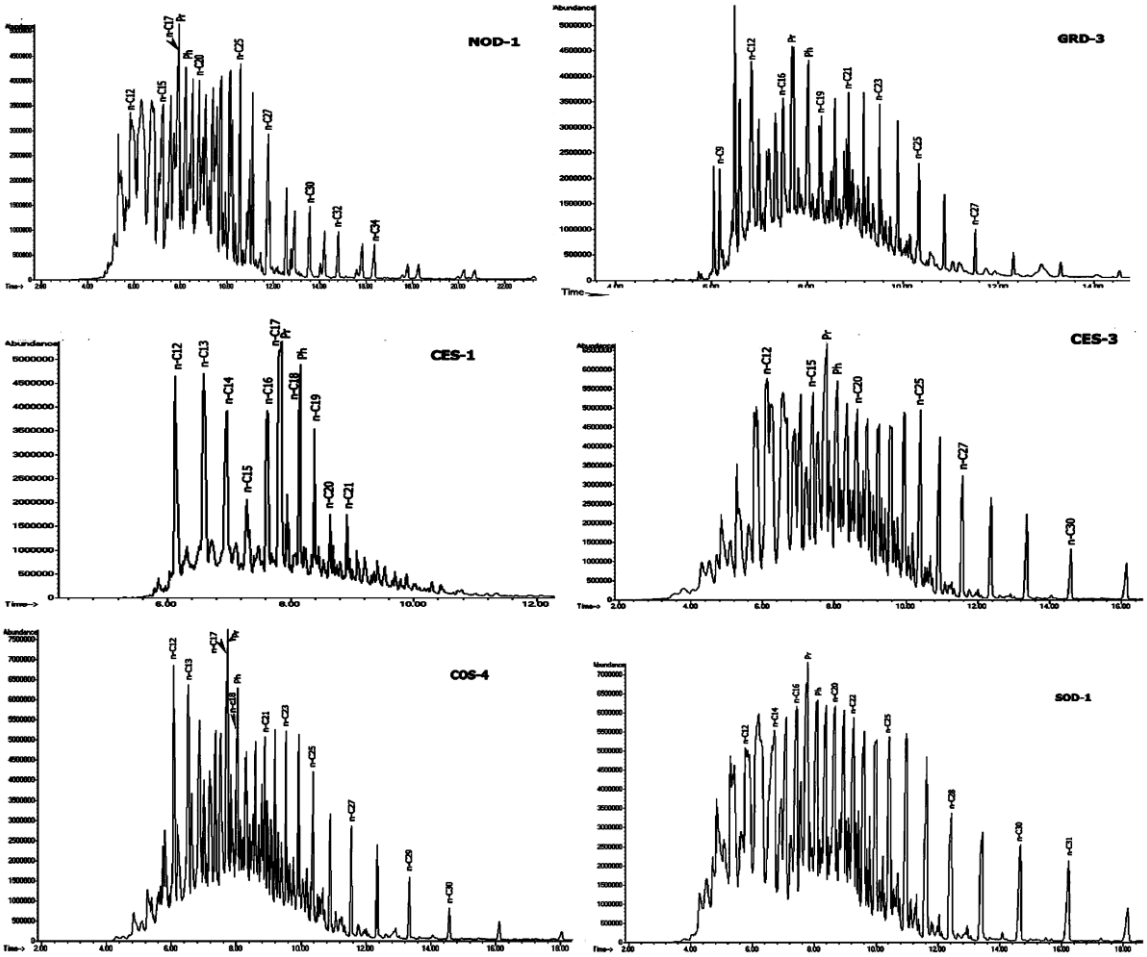

Figure 4. *Representative GC-MS chromatograms monitored on m/z 71; Pr = pristine and Ph = phytane.*

In contrast, samples exhibiting elevated concentrations of NSO compounds were classified as biodegraded crude oils, while those containing relatively high proportions of aromatic hydrocarbons were categorized as aromatic-intermediate crudes (Figure 5). The relative abundance of aromatic hydrocarbons in crude oil is primarily controlled by the type of source organic matter and the level of thermal maturity. However, because aromatic compounds are generally more resistant to biodegradation than saturated hydrocarbons, an apparent enrichment

Romanian Journal of Petroleum & Gas Technology
Vol. VII (LXXVIII) • No. 1/2026

in aromatics may also reflect selective microbial degradation of the saturated fraction [28]. Pristane and phytane are present in all samples, with pristane typically more abundant than phytane. Calculated Pr/Ph ratios fall within a relatively narrow range (Table 1), suggesting broadly similar redox conditions during organic matter deposition. Ratios of Pr/n-C_{17} and Ph/n-C_{18} show moderate variability among samples, reflecting subtle differences in maturity and/or secondary alteration rather than fundamentally distinct source inputs [26]. Cross-plots of Pr/n-C_{17} versus Ph/n-C_{18} (Figure 6) show that the samples cluster tightly within a restricted compositional field, with no distinct separation between oils from different depobelts.

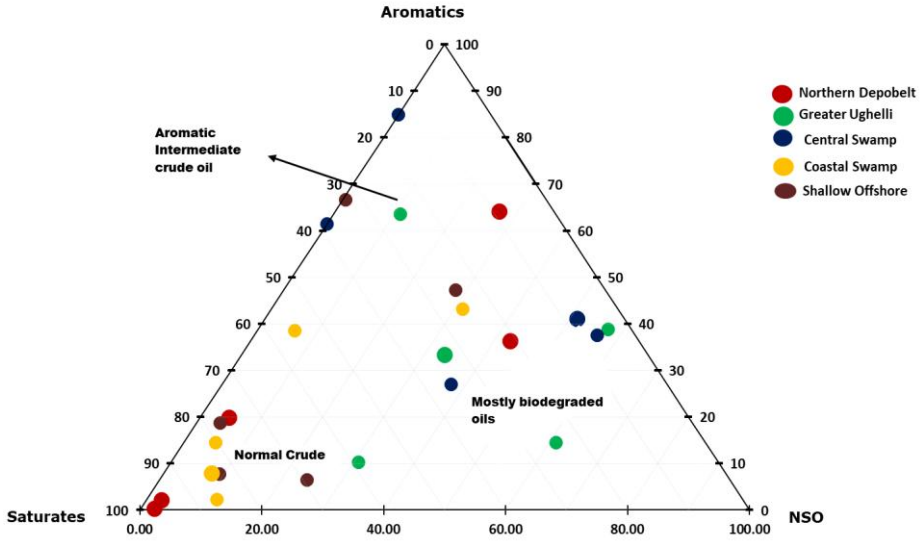

Figure 5. *Ternary diagram displaying the chemical contents (saturated, aromatics, and NSO fractions) of the analysed crude oil from the five depobelt of the Niger Delta* [27].

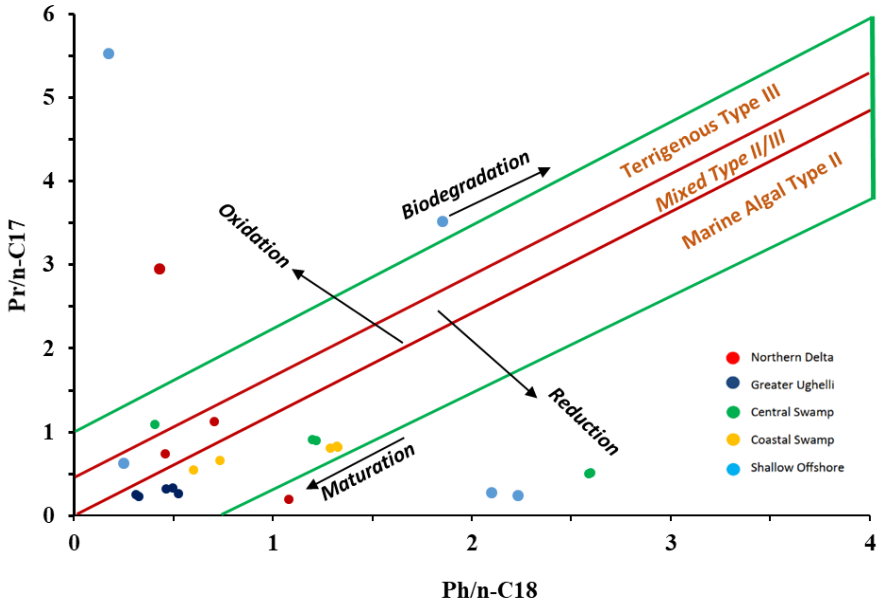

Figure 6*. A cross plotting of pristane/n-C_{17} vs phytane/n-C_{18} indicating Type II/III & Type II Kerogen, and deposition in slightly reducing condition; the arrow points to the upper right- direction indicates growing biodegradation, whereas the arrow points to the lower left-direction indicates increase in maturity [3].*

***Table 1**. The n-Alkane and acyclic isoprenoid ratios (m/z 71) of the crude oils*

Sample ID	Pr/Ph	Pr/n-C_{17}	Ph/n-C_{18}	CPI
Northern Depobelt				
NOD-1	3.87	2.95	0.43	1.17
NOD-2	0.75	0.19	1.08	1.14
NOD-3	1.76	1.12	0.71	1.05
NOD-4	1.90	0.74	0.46	1.03
NOD-5				
Greater Ughelli				
GRD-1	0.99	0.32	0.46	1.10
GRD-2	1.71	0.25	0.31	1.10
GRD-3	1.04	0.26	0.53	0.99
GRD-4	1.69	0.23	0.33	1.11
GRD-5	1.01	0.33	0.50	1.13
Central Swamp				
CES-1	2.08	0.90	1.20	0.92
CES-2	0.65	0.51	2.60	1.02
CES-3	0.63	0.50	2.59	1.01
CES-4	0.98	1.08	0.41	1.06
CES-5	2.01	0.89	1.22	1.03
Coastal Swamp				
COS-1	1.21	0.83	1.32	0.99
COS-2	1.01	0.54	0.60	0.68
COS-3	1.23	0.80	1.29	1.01
COS-4	1.57	0.66	0.73	0.93
COS-5	1.35	0.82	1.33	0.98
Shallow Offshore				
SOD-1	0.62	0.25	9.23	1.21
SOD-2	2.85	0.63	0.25	1.24
SOD-3	1.63	3.51	1.85	0.87
SOD-4	4.61	12.53	0.17	0.87
SOD-5	0.63	0.28	8.10	1.22

*Pr- Pristane, Ph- Phytane

*CPI- Carbon Preference Index = Odd number n-alkane/even number n-alkanes [29].

Biomarker Distributions and Molecular Signatures

GC–MS analysis of the saturated hydrocarbon fractions reveals closely comparable hopane and sterane distributions among the crude oil samples (Figure 7 and Figure 8). The m/z 191 mass chromatograms are dominated by C_{30} αβ-hopane, with well-developed C_{31}–C_{35} homohopanes showing a decreasing abundance trend toward higher carbon numbers (Figure 7). The homohopane distributions are generally consistent across samples, suggesting deposition under similar redox conditions (Table 2).

Romanian Journal of Petroleum & Gas Technology
Vol. VII (LXXVIII) • No. 1/2026

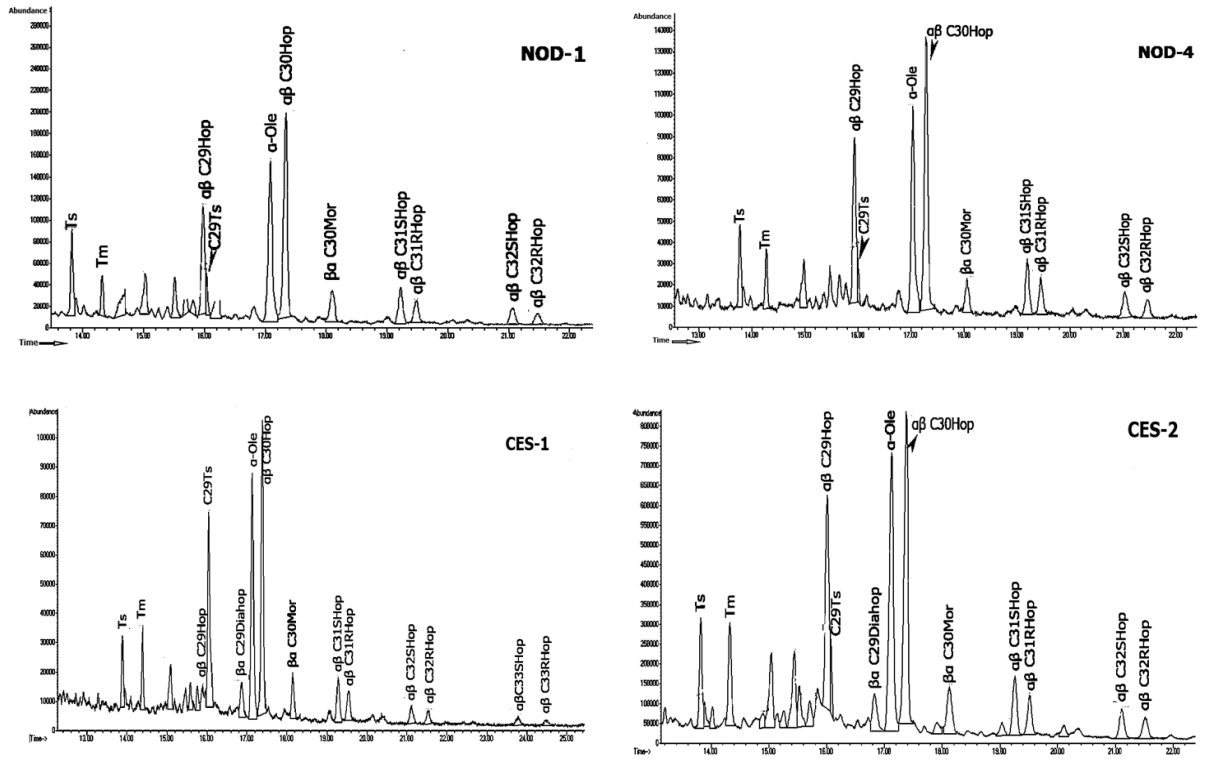

***Figure 7**. Representative m/z 191 mass chromatograms of selected crude oil samples.*

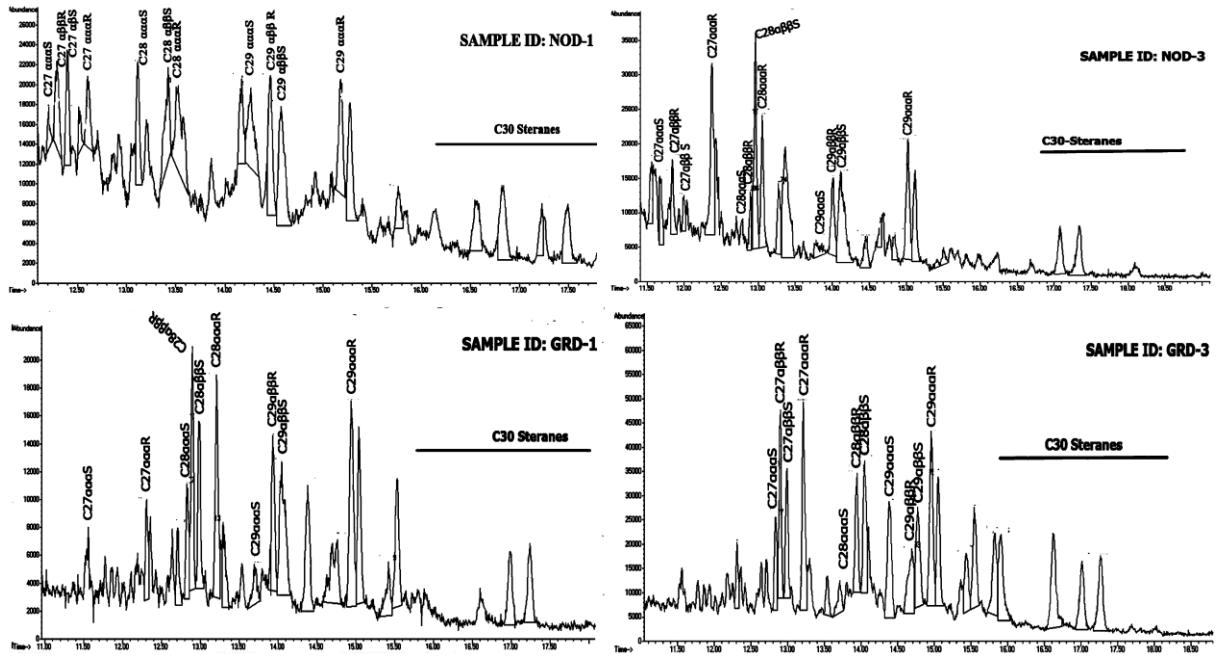

***Figure 8**. Representative m/z 217 mass chromatograms of selected crude oil samples*

The presence of oleanane in all samples, expressed as moderate oleanane/C_{30} hopane ratios, indicates a significant higher-plant organic matter contribution, consistent with a deltaic source environment. Ts/Tm ratios show limited variability, suggesting broadly comparable levels of thermal maturity. Sterane distributions (m/z 217) are characterized by mixed C_{27}–C_{29} components, with C_{29} steranes typically dominant or co-dominant (Figure 8). This pattern supports a mixed terrestrial–marine organic matter input for the oils. The relative consistency of sterane distributions across depobelts further supports genetic similarity among the crude oils analyzed (Table 3).

The examined crudes were originated from a mixture of algae and land plant organic matter deposited in a little anoxic (reducing) to oxic environment, according to a cross plot of C_{29}/C_{27} steranes vs Pr/Ph ratio (Figure 9) [30].The results of the analysis of the crude oils showed that the values of the C_{29}/C_{27} regular steranes for the Northern depobelt ranged from 1.00 to 1.70, for the Greater Ughelli from 1.12 to 1.53, for the Central Swamp from 1.00 to 3.78, for the Coastal Swamp from 0.46 to 1.69, and for the Shallow offshore from 0.95 to 1.84 (Table 3). These values represent sources from terrestrial (land plant) organic matter [11]. The peaks assignments for hopanes (m/z 191) and steranes (m/z 217) mass chromatograms are presented on Table 4.

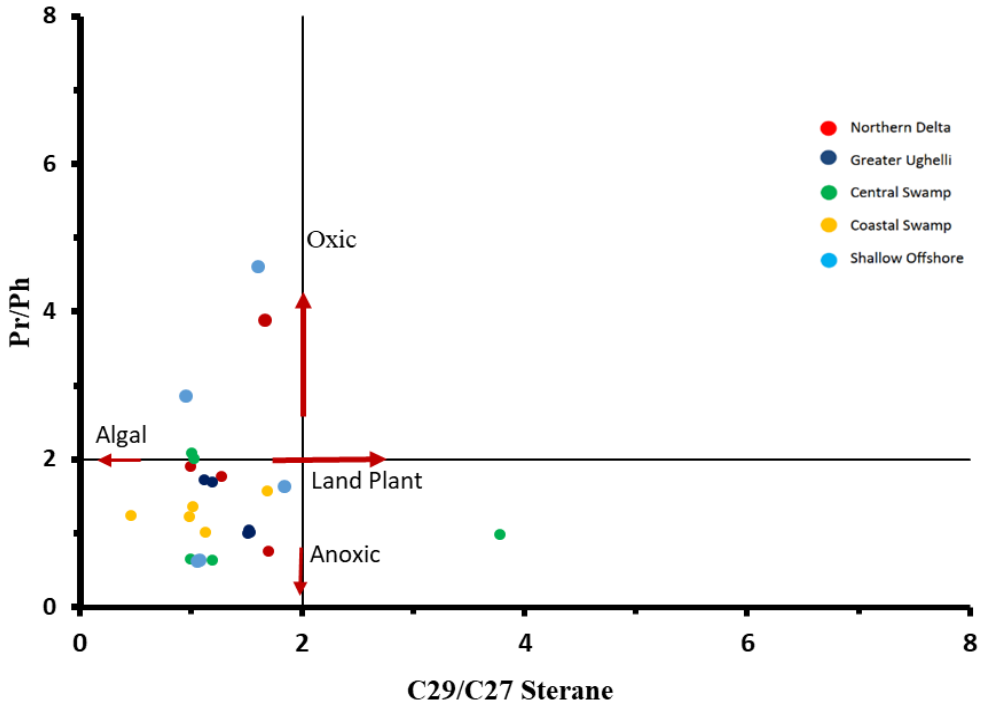

Figure 9. *Cross plot diagram of C_{29}/C_{27} steranes vs. Pr/Ph ratio; the plot indicated that oil samples were derived from algal/land plant organic matter with a slightly anoxic (reducing) to oxic condition of deposition* [30].

Romanian Journal of Petroleum & Gas Technology
Vol. VII (LXXVIII) • No. 1/2026

***Table 2**. Summary of key hopane ratios (m/z 191) for all analyzed samples*

SAMPLES	Ts/(Ts+Tm)	Ts/Tm	Oleanane Index	$C_{31}H/C_{30}H$	Mor./C_{30}Hop	$C_{29}/C_{30}H$	$C_{29}Ts/[C_{29}Hop + C_{29}Ts]$	Olea./(Olea. + C_{30} Hop.)	$C_{32}H$: 22S/(22 S + 22R)
Northern Depobelt									
NOD-1	0.66	2.28	0.89	0.34	0.21	0.5	0.16	0.5	0.6
NOD-2	0.54	1.16	0.39	0.34	0.17	0.62	0.07	0.28	0.58
NOD-3	0.70	2.36	0.97	0.33	0.2	0.49	0.14	0.47	0.58
NOD-4	0.59	1.41	0.75	0.36	0.13	0.54	0.1	0.43	0.57
NOD-5									
Greater Ughelli									
GRD-1	0.54	1.17	0.75	0.36	0.16	0.63	0.1	0.43	0.54
GRD-2	0.48	0.91	0.84	0.34	0.16	0.68	0.06	0.46	0.56
GRD-3	0.44	0.78	0.71	0.32	0.16	0.58	0.08	0.42	0.59
GRD-4	0.49	0.89	0.83	0.34	0.15	0.68	0.07	0.47	0.56
GRD-5	0.53	0.16	0.76	0.35	0.16	0.62	0.11	0.45	0.52
Central Swamp									
CES-1	0.45	0.81	0.91	0.32	0.16	0.08	0.9	0.48	0.57
CES-2	0.83	4.78	0.95	0.34	0.19	0.61	0.12	0.49	0.57
CES-3	0.50	0.99	0.64	0.39	0.24	0.5	0.1	0.39	0.57
CES-4	0.47	0.88	0.89	0.33	0.17	0.56	0.1	0.47	0.64
CES-5	0.48	0.82	0.93	0.35	0.16	0.12	0.89	0.5	0.55
Coastal Swamp									
COS-1	0.52	1.08	0.9	0.35	0.19	0.65	0.07	0.47	0.55
COS-2	0.43	0.74	0.9	0.34	0.19	0.58	0.12	0.47	0.58
COS-3	0.61	1.54	0.7	0.23	0.12	0.62	0.17	0.41	0.61
COS-4	0.50	1	0.39	0.33	0.17	0.65	0.11	0.28	0.59
COS-5	0.51	1.06	1.01	0.33	0.18	0.67	0.06	0.46	0.56
Shallow Offshore									
SOD-1	0.60	1.47	0.43	0.29	0.23	0.62	0.08	0.3	0.6
SOD-2	0.52	1.09	0.99	0.29	0.26	0.68	0.09	0.5	0.59
SOD-3	0.51	1.06	4.67	0.27	0.17	0.33	0.36	0.82	0.58
SOD-4	0.53	1.08	4.76	0.3	0.18	0.36	0.28	0.89	0.56
SOD-5	0.55	1.5	0.42	0.3	0.22	0.65	0.06	0.35	0.6

Romanian Journal of Petroleum & Gas Technology
Vol. VII (LXXVIII) • No. 1/2026

Table 3. *Summary of key sterane ratios for all analyzed samples*

SAMPLES	C_{27}/C_{29} Ster.	C_{28}/C_{29} Ster.	C_{29}/C_{28} Ster.	C_{29}/C_{27} Ster.	C_{29}:20S/(20S+20R)	Ster./Hop	Hop/Ster.	Steranes Index	$\%C_{30}$ Ster.
Northern Depobelt									
NOD-1	0.60	0.94	1.07	1.67	0.81	0.14	7.01	0.21	21.35
NOD-2	0.59	0.39	2.57	1.70	0.37	0.06	16.55	0.35	35.00
NOD-3	0.78	0.91	1.10	1.28	0.17	0.19	5.37	0.19	18.85
NOD-4	1.00	0.70	1.43	1.00	0.47	0.13	7.70	0.16	16.11
NOD-5	-	-	-	-	-	-	-	-	-
Greater Ughelli									
GRD-1	0.66	0.93	1.08	1.51	0.49	0.19	5.14	0.10	9.98
GRD-2	0.89	0.79	1.27	1.12	0.53	0.14	7.01	0.24	23.97
GRD-3	0.65	0.92	1.06	1.52	0.50	0.18	5.13	0.11	10.10
GRD-4	0.87	0.81	1.25	1.19	0.51	0.15	6.81	0.21	21.88
GRD-5	0.67	0.90	1.04	1.53	0.52	0.18	5.21	0.11	10.01
Central Swamp									
CES-1	0.99	0.52	1.93	1.01	0.29	0.16	6.39	0.24	24.42
CES-2	1.00	0.62	1.61	1.00	0.61	0.20	5.05	0.20	19.57
CES-3	0.84	0.76	1.31	1.19	0.46	0.36	2.80	0.09	8.89
CES-4	0.26	0.56	1.79	3.78	0.44	0.15	6.50	0.26	26.41
CES-5	0.98	0.53	1.90	1.03	0.41	0.19	6.51	0.23	24.31
Coastal Swamp									
COS-1	1.01	0.58	1.73	0.99	0.49	0.21	4.79	0.20	20.31
COS-2	0.88	0.54	1.85	1.13	0.28	0.16	6.12	0.23	22.68
COS-3	2.15	1.14	0.88	0.46	0.79	0.51	1.94	0.07	7.24
COS-4	0.59	0.45	2.23	1.69	0.07	0.31	3.18	0.11	11.03
COS-5	1.03	0.56	1.69	1.02	0.50	0.22	4.76	0.21	20.29

Shallow Offshore									
SOD-1	0.94	1.07	0.93	1.06	0.43	0.09	11.55	0.20	20.03
SOD-2	1.05	1.53	0.66	0.95	0.56	0.28	3.57	0.15	15.12
SOD-3	0.54	0.53	1.89	1.84	0.72	0.07	14.15	0.43	42.60
SOD-4	0.56	0.55	1.91	1.60	0.70	0.09	15.01	0.45	30.20
SOD-5	0.89	1.06	0.86	1.08	0.42	0.10	7.01	0.21	20.01

*C_{29}: 20S / (20s+20R) - C29 αα 20S stigmastanes/(C_{29} αα 20S stigmastanes + C_{29} αα 20R stigmastanes)

*Oleananes index (Olea. Index) - α-oleananes/ C_{30} 17α (H)-hopanes

*Steranes Indexes - C_{30} Steranes/ Σ (C_{27} regular Steranes – C_{30} Steranes)

Ts/(Ts+Tm): 18α(H)-trisnorhopanes /(18α(H)-trisnorhopan +17α(H)-trisnorhopanes)

Ts/Tm: 18α(H)-trisnorhopanes/17α(H)-trisnorhopanes

C_{31}H/C_{30}H- C_{31}-17a(H), 21b(H)-30 homohopanes (22S+22R)/2/ (C30 17α (H)-hopanes)

Mor./C_{30}Hop- C_{30}-17b(H), 21a(H)-moretanes/ C_{30} 17α (H)-hopanes

C_{29}/C_{30}H- C_{29} Tm 17a(H)21b(H)-norhopanes/C_{30} 17α (H)-hopanes

C_{29}Ts/[C29Hop + C_{29}Ts]- C_{29}-18a(H) norneohopanes ($_{29}$Ts)/ (C_{29} Tm 17a(H)21b(H)-norhopanes+ C_{29} -18a (H) norneohopanes (29Ts))

Olea./(Olea. + C_{30} Hop.)- 18α (H) –oleananes/(18α (H) –oleananes + C_{30} 17α (H)-hopanes)

*C_{32}H: 22S/(22S + 22R) - C_{32}-17a(H), 21b(H)-30 bishomohopanes (22S)/ (C32-17a(H), 21b(H)-30 bishomohopanes (22S)+ C_{32}-17a(H), 21b(H)-30 bishomohopanes (22R)

* Ster./Hop. - Regular Steranes /17α-hopanes

* Ster : Steranes

* Hop: Hopanes

%C_{27} -Sterane

%C_{28} -Steranes

%C_{29} -Sterane

%C_{30}- Steranes

Table 4. *Peaks assignments on m/z 191 (hopanes) and m/z 217 (steranes) mass chromatograms*

Peak	***Compound name***
Ts	18α(H)- trisnorneohopane
Tm	17α(H)-trisnorhopane
αβC29Hop	C29 Tm 17a(H)21β(H)-norhopane
C29Ts	C29-18α(H) norneohopane (29Ts)
βαC29Diahop	C29-17α(H), 21β(H)-25-dinorhopane
α -ole	18α (H) -oleanane
αβC30Hop	C30 17α (H)-hopane
βαC30Mor	C30-17β(H), 21α(H)-moretane
αβC31SHop	C31-17α(H), 21β(H)-30 homohopane (22S)
αβC31RHop	C31-17α(H), 21β(H)-30 homohopane (22R)
αβC32SHop	C32-17α(H), 21β(H)-30 bishomohopane (22S)
αβC32RHop	C32-17α(H), 21β(H)-30 bishomohopane (22R)
C27ααaS	C27 5α(H) 14α(H) 17a(H) cholestane (20S)
C27αββR	C27 13β(H) 17α(H) Diacholestane (20R)
C27αββS	C27 5α(H) 14β(H) 17β(H) cholestane (20S)
C27αααR	C27 5α(H) 14α(H) 17α(H) cholestane (20R)
C28ααaS	C28 5α(H) 14α(H) 17a(H) ergostane (20S)
C28αββR	C28 5α(H) 14β(H) 17β(H) cholestane (20R)
C28αββS	C28 5α(H) 14β(H) 17β(H) cholestane (20S)
C28αααR	C28 5α(H) 14α(H) 17α(H) ergostane (20R)
C29ααaS	C29 5α(H) 14α(H) 17α(H) stigmastane (20S)
C29αββR	C29 5α(H) 14β(H) 17β(H) stigmastane (20R)
C29αββS	C29 5α(H) 14β(H) 17β(H) stigmastane (20S)
C29αααR	C29 5α(H) 14α(H) 17α(H) stigmastane (20R)

Maturity is known to have a considerable impact on the Ts/(Tm+Ts), where the Ts is more thermally stable than the Tm. According to [40] the C_{29}:20S/(20S + 20R) steranes ratio rises as thermal maturity increases. It does so from 0.0 to around 0.5 (0.52-0.55= achieving equilibrium) when maturity develops further [3],[31],[32]. At or close to the apex of the oil generating window, the C_{29}: 20S/(20S+20R) ratio approaches its equilibrium point [11]. Normal equilibrium for the C_{29}: 20S/(20S+20R) ratio will be maintained after the peak of the oil-generating window. The C_{29}:20S/(20S+20R) ratio ranges from 0.17 to 0.81 for oil samples from the Northern Depobelt, from 0.49 to 0.53 for those from Greater Ughelli, from 0.29 to 0.61 for the Central Swamp, from 0.07 to 0.79 for the Coastal Swamp, and from 0.42-0.72 for those from Shallow Offshore (Table 2). However, as maturity develops, the Ts / (Ts+Tm) ratio increases as well, even after the peak is achieved [11]. It achieves its endpoint at or near the end of the oil generative window. As equilibrium is attained in the C_{29}: 20S/ (20S+20R) ratio, the values will stay constant [11],[32]. The range of Ts/Ts+Tm values for the Northern depobelt is 0.54-0.70; for Greater Ughelli, the values were 0.43-0.54; for Central Swamp, the values were 0.45-0.83; for Coastal Swamp, the values were 0.42-0.61; and for Shallow Offshore, the values were 0.51-0.60. The maturity of the samples is shown by a cross plot of Ts/(Ts + Tm) and C_{29}: 20S/(20S + 20R) regular sterane of the examined crude oils (Figure 10).

Romanian Journal of Petroleum & Gas Technology
Vol. VII (LXXVIII) • No. 1/2026

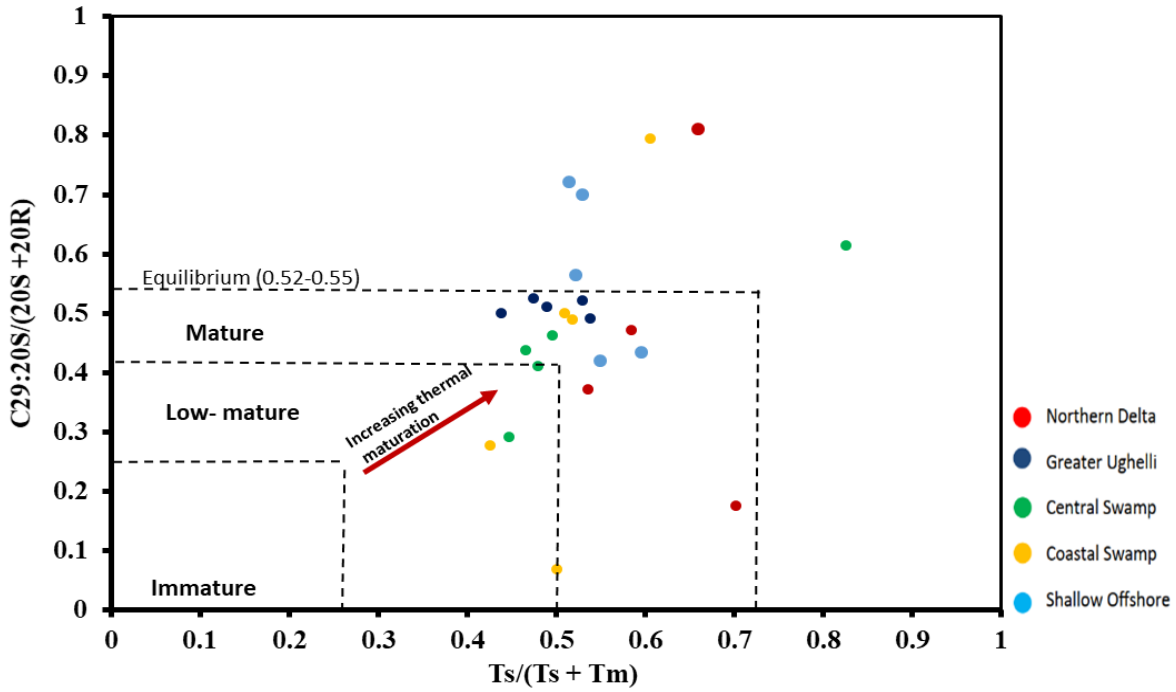

Figure 10. *A cross plot of Ts/ (Ts + Tm) and C_{29} 20S/(20S + 20R) regular sterane of the analyzed crude oils, demonstrating the maturity of the samples. The ratios on the axes increase with maturity.*

Hierarchical Cluster Analysis (HCA)

Hierarchical cluster analysis (HCA) was carried out on the standardized biomarker and bulk geochemical dataset using Ward's method and Euclidean distance to evaluate genetic relationships among the investigated crude oils and to assess reservoir continuity. The resulting dendrogram is presented in Figure 11. The dendrogram shows that the majority of samples merge at relatively low rescaled linkage distances, indicating strong compositional similarity across the dataset. Most oils coalesce into a dominant cluster before a rescaled distance of approximately 15, reflecting a high degree of genetic relatedness. Importantly, samples from different depobelts are interspersed within the same clusters rather than forming geographically isolated groupings. For example, samples from the Coastal Swamp, Greater Ughelli, Northern Delta, Central Swamp, and Shallow Offshore depobelts occur within common sub-branches. This intermixing demonstrates that geographic or structural separation does not correspond to geochemical segregation. Minor sub-clusters are present within the main grouping, but these merge at only slightly higher linkage distances. The limited separation suggests subtle internal variability rather than the existence of distinct oil families. Such variability may reasonably be attributed to minor differences in thermal maturity, migration fractionation, or small-scale facies heterogeneity within a broadly similar source rock system [3],[9],[33]. The absence of isolated branches at high linkage distance confirms that no sample exhibits a fundamentally different biomarker signature. Consequently, the HCA strongly supports the presence of a single dominant petroleum system with extensive lateral continuity across the study area.

Romanian Journal of Petroleum & Gas Technology
Vol. VII (LXXVIII) • No. 1/2026

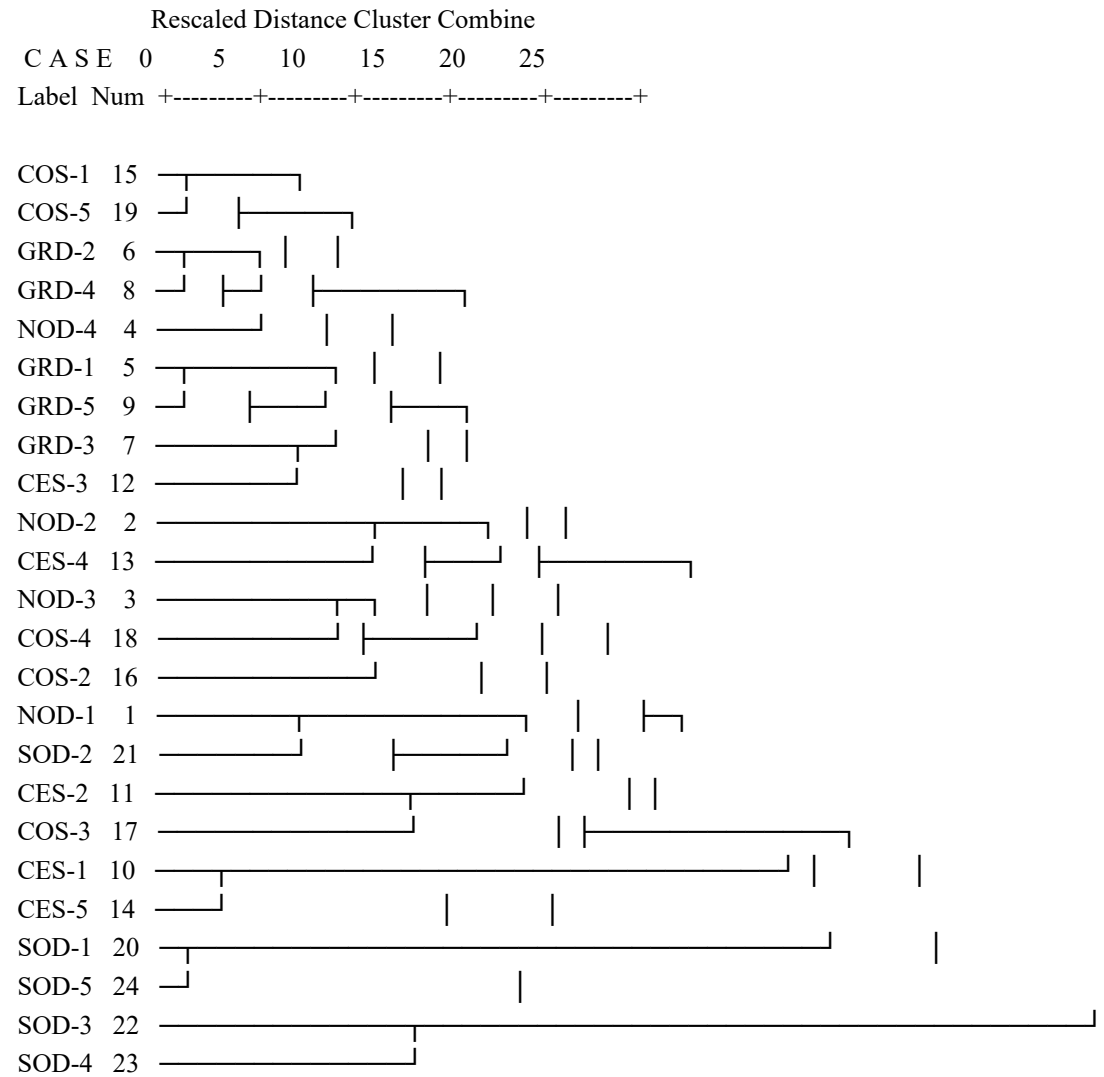

***Figure 11**. Dendrogram of hierarchical cluster analysis based on standardized biomarker parameters*

Principal Component Analysis (PCA)

Principal component analysis (PCA) was applied to the same standardized dataset to quantify the dominant sources of variance and to identify the geochemical processes controlling oil composition. The scree plot and eigenvalue distribution are presented in Figure 12 and Table 5, respectively. Five principal components with eigenvalues greater than or equal to one were extracted, collectively explaining 79.48% of the total variance. The first principal component (PC1) accounts for 35.77% of the variance and therefore represents the most significant geochemical control in the dataset. PC2 explains 13.74%, PC3 12.63%, PC4 9.52%, and PC5 7.83% of the total variance. The scree plot displays a distinct inflection after the fifth component, confirming that additional components contribute only marginal explanatory power.

Romanian Journal of Petroleum & Gas Technology
Vol. VII (LXXVIII) • No. 1/2026

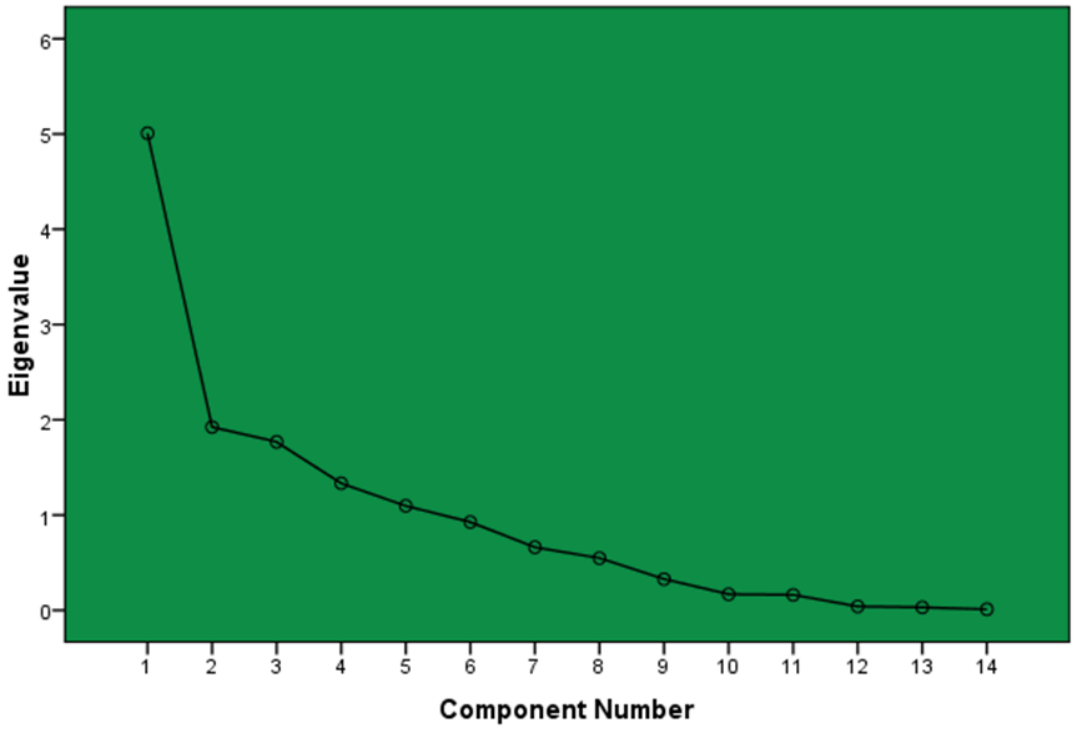

***Figure 12**. Principal component scree plot*

***Table 5.** Total Variance Explained*

	Initial Eigenvalues			Extraction Sums of Squared Loadings		
Component	**Total**	**% of Variance**	**Cumulative %**	**Total**	**% of Variance**	**Cumulative %**
1	5.008	35.773	35.773	5.008	35.773	35.773
2	1.923	13.739	49.511	1.923	13.739	49.511
3	1.768	12.627	62.138	1.768	12.627	62.138
4	1.333	9.518	71.657	1.333	9.518	71.657
5	1.096	7.826	79.483	1.096	7.826	79.483
6	0.926	6.612	86.095			
7	0.662	4.727	90.822			
8	0.547	3.910	94.732			
9	0.327	2.337	97.070			
10	0.168	1.201	98.271			
11	0.161	1.153	99.424			
12	0.040	0.286	99.710			
13	0.030	0.215	99.924			
14	0.011	0.076	100.000			

Communalities

The communalities indicate the proportion of variance in each variable explained by the extracted components. These values range from 0.507 to 0.944, demonstrating that the five-component solution adequately represents the majority of the dataset variability. Variables such as Pr/(Pr+Ph), Pr/Ph, Olea. Index, and Olea. /(Olea. +C_{30} Hop.) exhibit particularly high communalities (>0.90), confirming that redox-sensitive and angiosperm-derived biomarker ratios dominate the multivariate structure. Even the lowest communality (C_{29}Ts/[C_{29}Hop + C_{29}Ts] at 0.507) remains acceptable, indicating that no variable is poorly represented (Table 6).

Table 6. *Communalities*

	Initial	**Extraction**
Pr/Ph	1.000	0.932
Pr/(Pr + Ph)	1.000	0.944
Pr/n-C_{17}	1.000	0.821
Ph/n-C_{18}	1.000	0.739
CPI	1.000	0.859
C_{29}/C_{27} Ster.	1.000	0.830
C_{29}: 20S/(20S+20R)	1.000	0.694
Ster./Hop	1.000	0.856
Ster. Index	1.000	0.881
Ts/(Ts+Tm)	1.000	0.577
Olea. Index	1.000	0.939
C_{29}Ts/[C_{29}Hop + C_{29}Ts]	1.000	0.507
Olea./(Olea. + C_{30} Hop.)	1.000	0.929
C_{32}H: 22S/(22S + 22R)	1.000	0.620

Interpretation of the Rotated Component Matrix

Varimax rotation was applied to enhance interpretability of the component structure. The rotated component matrix is presented in Table 7. The first principal component (PC1) is characterized by strong positive loadings of Olea. Index (0.930), Olea./(Olea.+C30 Hop.) (0.884), Pr/n-C17 (0.789), and Ster. Index (0.670). These parameters are widely recognized as indicators of terrestrial organic matter input and higher-plant contribution, particularly angiosperm-derived material. PC1 is therefore interpreted as representing source facies and organic matter provenance. Its dominance in the variance structure indicates that variations in terrestrial input constitute the primary control on compositional differences among the oils.

The second principal component (PC2) is strongly influenced by Pr/(Pr+Ph) (0.926) and Pr/Ph (0.864), with a significant negative loading from Ph/n-C18 (-0.634). These ratios are sensitive to depositional redox conditions, suggesting that PC2 captures variability related to oxic versus suboxic–anoxic depositional environments. However, dispersion along PC2 is limited, indicating that redox conditions across the studied oils were broadly similar and do not define separate oil families. The third principal component (PC3) shows strong positive loadings for Ts/(Ts+Tm) (0.751), C_{29} 20S/(20S+20R) (0.622), and CPI (0.623). These parameters are widely

used maturity indicators, reflecting isomerization and thermal evolution. PC3 is therefore interpreted as a thermal maturity axis. The relatively modest variance explained by PC3 indicates that maturity differences are present but not sufficiently large to subdivide the oils into distinct populations. The fourth principal component (PC4) is dominated by a strong negative loading of Ster./Hop (-0.903), accompanied by a positive contribution from Ster. Index (0.630). This component likely reflects variations related to sterane–hopane balance, which may be influenced by migration fractionation, subtle facies shifts, or secondary alteration processes. Its contribution to overall variance is comparatively small, suggesting that such effects are subordinate. The fifth principal component (PC5) is characterized by high positive loadings of C_{29}/C_{27} Ster. (0.803) and $C_{32}H$ 22S/(22S+22R) (0.770). These parameters provide additional discrimination of source input proportions and hopane isomerization equilibrium. PC5 captures subtle compositional nuances but explains less than 8% of the total variance, indicating limited geological significance relative to PC1 and PC2.

***Table** 7. Rotated Component Matrix*

	Component				
	1	**2**	**3**	**4**	**5**
Pr/Ph	0.383	0.864	0.152	0.118	-0.046
Pr/(Pr + Ph)	0.266	0.926	-0.023	0.043	-0.118
Pr/n-C17	0.789	0.398	0.097	0.172	0.035
Ph/n-C18	-0.139	-0.634	0.391	0.403	-0.046
CPI	-0.602	0.097	0.623	0.283	0.142
C29/C27 Ster.	0.123	0.088	-0.309	0.259	0.803
C29: 20S/(20S+20R)	0.490	0.190	0.622	-0.170	0.051
Ster./Hop	-0.184	0.015	0.062	-0.903	-0.049
Ster. Index	0.670	0.120	-0.106	0.630	0.103
Ts/(Ts+Tm)	0.013	-.084	0.751	-0.052	-0.047
Olea. Index	0.930	0.201	-0.005	0.185	-0.018
C29Ts/[C29Hop + C29Ts]	0.131	0.301	-0.363	0.236	-0.460
Olea./(Olea. + C30 Hop.)	0.884	0.357	0.009	0.112	-0.084
C32H: 22S/(22S + 22R)	-0.062	-0.083	0.124	-0.024	0.770

Extraction Method: Principal Component Analysis. Rotation Method: Varimax with Kaiser Normalization. a. Rotation converged in 7 iterations.

PCA Score Plot and Genetic Implications

The PCA score plot for PC1 versus PC2 is shown in Figure 13. The score distribution reveals strong clustering of samples irrespective of depobelt classification. Oils from different structural provinces overlap extensively within the multivariate space, forming a compact grouping without discrete separation fields. The absence of clearly separated clusters in the score plot reinforces the dendrogram interpretation that the oils belong to a single dominant genetic family. Limited dispersion along PC3 further supports the interpretation of minor maturity gradients rather than distinct petroleum systems.

Romanian Journal of Petroleum & Gas Technology
Vol. VII (LXXVIII) • No. 1/2026

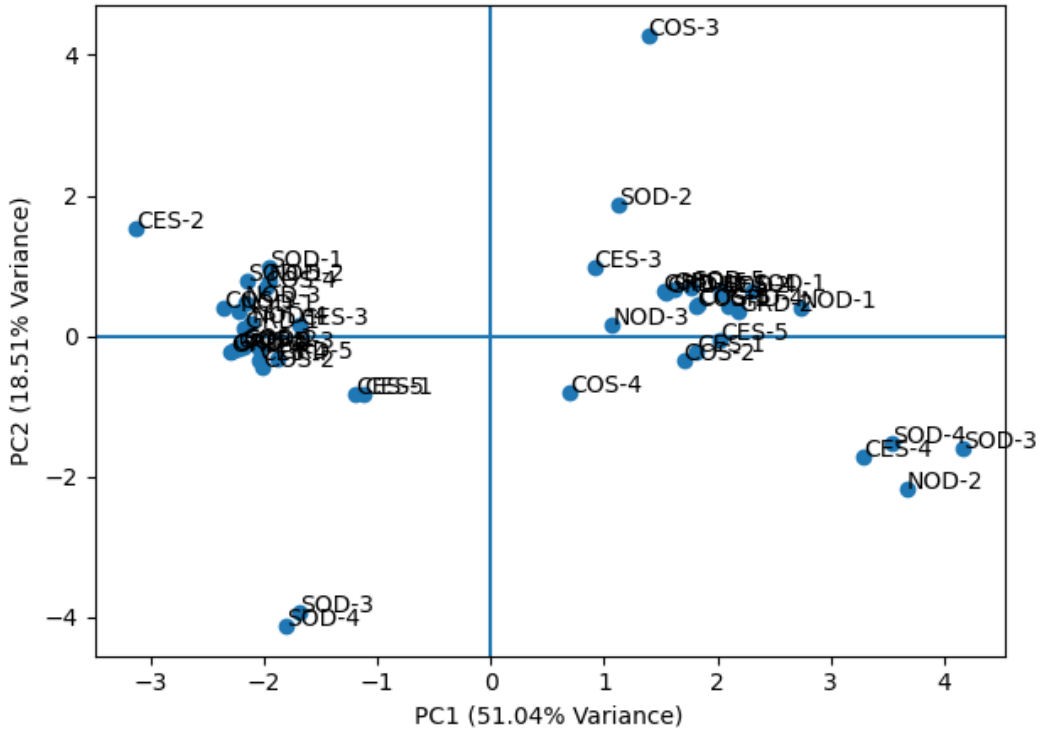

***Figure 13**. Principal Component Analysis (PCA) score plot of PC1 versus PC2 derived from standardized biomarker parameters of the analyzed crude oil samples*

Correlation Structure

The correlation matrix (Table 8) further clarifies the internal relationships among variables. Strong positive correlations between Pr/Ph and Pr/(Pr+Ph) ($r = 0.929$), as well as between Olea. Index and Olea./(Olea.+C30 Hop.) ($r = 0.939$), confirm redundancy among terrestrial and redox-sensitive proxies. Similarly, strong associations between Ster. Index and Olea. Index ($r = 0.741$) reinforce the linkage between sterane distributions and higher-plant input. Negative correlations between Ph/n-C18 and Pr-based ratios are consistent with redox differentiation trends. The high degree of inter-correlation among source-related biomarkers explains the dominance of PC1 and PC2 in the PCA structure.

Star (Radar) Plot Comparisons

Star plots constructed from selected diagnostic biomarker ratios provide a visual comparison of oil fingerprints across depobelts. The composite radar diagram is shown in Figure 14, while depobelt-specific radar plots are presented in Figure 15. The radar plots display highly similar polygonal geometries among samples. The overlapping shapes indicate near-identical relative proportions of key biomarker ratios across the study area. Although minor deviations are observed in certain axes such as Ts/(Ts+Tm) and CPI, these differences are subtle and do not alter the overall fingerprint architecture. The visual coherence of the radar diagrams corroborates the statistical findings from HCA and PCA, demonstrating that the oils share a common geochemical signature.

Romanian Journal of Petroleum & Gas Technology
Vol. VII (LXXVIII) • No. 1/2026

Table 8. *Correlation Matrix*

		Pr/Ph	Pr/(Pr + Ph)	Pr/n-C17	Ph/n-C18	CPI	C29/C27 Ster.	C29: 20S/(20S +20R)	Ster./ Hop	Ster. Index	Ts/(Ts +Tm)	Olea. Index	C29Ts/[C29 Hop+C29Ts]	Olea./(Olea. + C30 Hop.)	C32H: 22S/(22S + 22R)
Correlation	**Pr/Ph**	1.000	0.929	0.749	-0.407	-0.079	0.010	0.357	-0.134	0.404	0.026	0.533	0.281	0.628	-0.046
	Pr/(Pr + Ph)	0.929	1.000	0.563	-0.556	-0.133	-0.018	0.226	-0.068	0.306	-0.081	0.458	0.368	0.579	-0.114
	Pr/n-C17	0.749	0.563	1.000	-0.173	-0.334	0.165	0.383	-0.242	0.643	0.028	0.829	0.165	0.799	-0.057
	Ph/n-C18	-0.407	-0.556	-0.173	1.000	0.351	-0.204	-0.065	-0.195	-0.017	0.208	-0.166	-0.095	-0.314	0.267
	CPI	-0.079	-0.133	-0.334	0.351	1.000	-0.014	0.159	-0.072	-0.273	0.296	-0.444	-0.281	-.0430	0.104
	C29/C27 Ster.	0.010	-0.018	0.165	-0.204	-0.014	1.000	-0.076	-0.322	0.315	-0.208	0.177	-0.110	0.141	0.395
	C29: 20S/(20S+20R)	0.357	0.226	0.383	-0.065	0.159	-0.076	1.000	0.065	0.186	0.257	0.434	-0.087	0.508	0.020
	Ster./Hop	-0.134	-0.068	-0.242	-0.195	-0.072	-0.322	0.065	1.000	-0.682	0.062	-0.308	-0.071	-0.264	0.114
	Ster. Index	0.404	0.306	0.643	-0.017	-0.273	0.315	0.186	-0.682	1.000	-0.092	0.741	0.264	0.661	0.040
	Ts/(Ts+Tm)	0.026	-0.081	0.028	0.208	0.296	-0.208	0.257	0.062	-0.092	1.000	-0.045	-0.212	-0.020	0.076
	Olea. Index	0.533	0.458	0.829	-0.166	-0.444	0.177	0.434	-0.308	0.741	-0.045	1.000	0.224	0.939	-0.110
	C29Ts/[C29Hop + C29Ts]	0.281	0.368	0.165	-0.095	-0.281	-0.110	-0.087	-0.071	0.264	-0.212	0.224	1.000	0.299	-.0171
	Olea./(Olea. + C30 Hop.)	0.628	0.579	0.799	-0.314	-0.430	0.141	0.508	-0.264	0.661	-0.020	0.939	0.299	1.000	-0.185
	C32H: 22S/(22S + 22R)	-0.046	-0.114	-0.057	0.267	0.104	0.395	0.020	0.114	0.040	0.076	-0.110	-0.171	-0.185	1.000

Romanian Journal of Petroleum & Gas Technology
Vol. VII (LXXVIII) • No. 1/2026

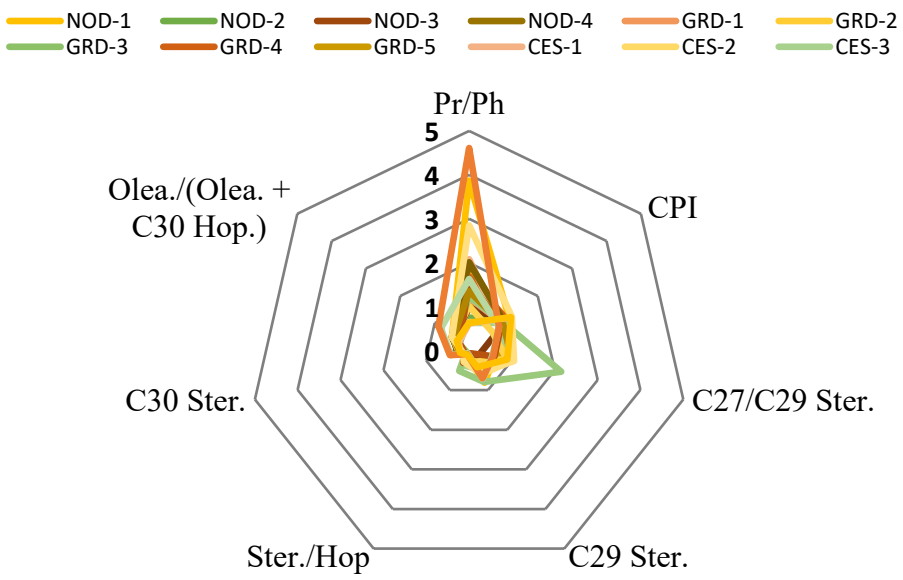

Figure 14. *Radar diagram comparing the values of selected biomarkers for the analysed crude oils.*

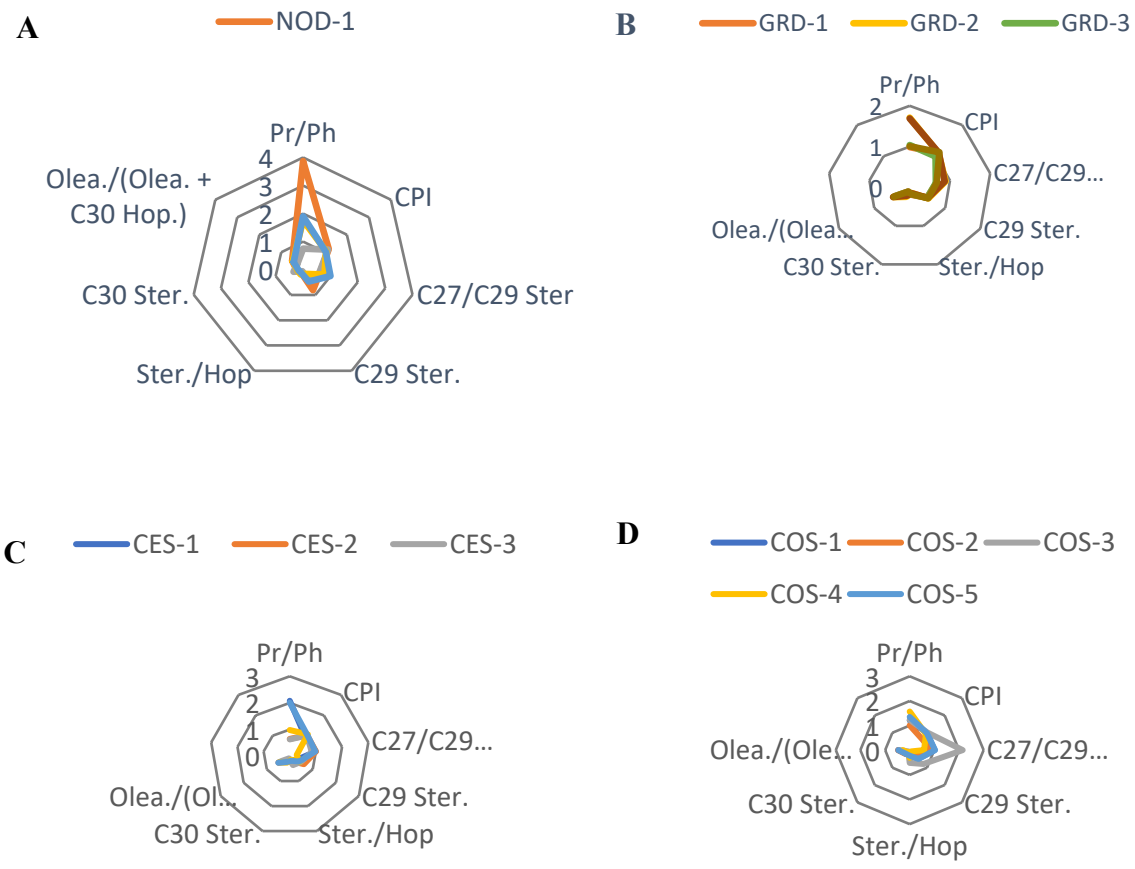

Romanian Journal of Petroleum & Gas Technology
Vol. VII (LXXVIII) • No. 1/2026

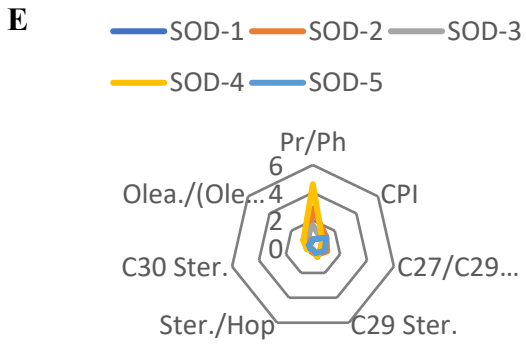

***Figure 15**. Depobelt-Specific Radar Plots comparing the values of selected biomarker for the studied oils: A. Radar plot for Northern Delta; B. Radar plot for Greater Ughelli; C. Radar plot for Central Swamp; D. Radar plot for Coastal Swamp; E. Radar plot for Shallow Offshore oil.*

Integrated Interpretation for Reservoir Continuity

The combined multivariate statistical analyses provide consistent and mutually reinforcing evidence for reservoir continuity. The hierarchical clustering demonstrates that all samples belong to a single dominant cluster with only minor internal subdivision. PCA reveals that the majority of compositional variance is controlled by terrestrial organic matter input and depositional redox conditions, with maturity and secondary effects playing subordinate roles. The absence of discrete separation in PCA score space and the strong overlap in radar plot fingerprints confirm that no genetically distinct oil populations are present. The results indicate that the studied crude oils are genetically homogeneous and derived from a common source facies within a unified petroleum system. The high degree of compositional similarity across depobelts supports effective lateral charge distribution and reservoir communication at the basin scale. Such statistical coherence is consistent with regional hydrocarbon migration pathways and limited compartmentalization within the producing intervals.

DISCUSSIONS

Oil Family Relationships and Source Rock Characteristics

The chromatographic patterns and biomarker distributions indicate that the analyzed crude oils share a high degree of genetic similarity. The dominance of well-resolved n-alkanes with minimal unresolved complex mixture suggests limited biodegradation and broadly comparable post-accumulation histories across the sampled reservoirs. Consistent Pr/Ph ratios and narrow ranges of Pr/n-C_{17} and Ph/n-C_{18} values further imply similar depositional redox conditions and overlapping maturity windows [34]. Biomarker signatures provide stronger evidence for a common petroleum system. The widespread occurrence of oleanane, together with mixed C_{27}–C_{29} sterane distributions dominated by C_{29} steranes, indicates significant higher-plant organic matter input deposited under deltaic to shallow-marine conditions. These characteristics are consistent with oils sourced predominantly from the organic-rich marine shales of the Akata Formation, with possible secondary contributions from interbedded Agbada shales, as widely reported for the Niger Delta Basin [13],[14],[15]. The relatively uniform Ts/Tm ratios and homohopane distributions suggest that the oils were generated within a comparable thermal maturity range, likely corresponding to peak oil generation in the deeper parts of the basin.

Minor variations observed in some samples are insufficient to define distinct oil families and are more plausibly attributed to subtle maturity differences or migration fractionation [9],[18]. These geochemical characteristics support the existence of a single dominant oil family across the investigated depobelts.

The dendrogram in Figure 11 also demonstrates that the analyzed oils coalesce into a single dominant cluster at relatively low linkage distances. In petroleum geochemical classification, low rescaled distance merging indicates strong similarity in biomarker distributions and bulk compositional attributes, implying shared genetic origin [3]. The absence of isolated clusters or late-merging branches suggests that none of the samples exhibits a significantly divergent biomarker signature. Samples from different depobelts are interspersed within the same cluster branches rather than forming geographically segregated groups. If separate source kitchens or isolated petroleum systems were present, one would expect discrete clustering patterns corresponding to structural or stratigraphic domains [35]. Instead, the dendrogram structure indicates extensive geochemical homogeneity across the study area. Minor sub-clusters observed within the primary grouping likely reflect subtle geochemical variations. Such variations can arise from slight maturity differences, minor facies heterogeneity within a broadly similar source rock, or secondary migration-related fractionation [3]. However, these internal subdivisions do not achieve sufficient linkage distance separation to justify recognition of distinct oil families. Consequently, the HCA results strongly support the interpretation of a single dominant oil family, implying regional-scale charge from genetically related source intervals and effective lateral communication within the reservoir system.

Multivariate Statistical Controls on Oil Composition and Variability

The application of hierarchical cluster analysis (HCA) and principal component analysis (PCA) provides an objective and quantitative framework for evaluating compositional similarities among the crude oils [2],[4],[9]. HCA reveals tight clustering of most samples at low linkage distances, with oils from different depobelts frequently grouping together. This pattern demonstrates that genetic affinity is not constrained by present-day structural compartmentalization or geographic separation. PCA further elucidates the dominant controls on compositional variability. The first principal component, which accounts for the largest proportion of variance, is primarily influenced by sterane distributions and oleanane-related parameters, indicating that source organic matter input and depositional environment are the primary factors governing oil composition. The second principal component reflects variations related to thermal maturity and minor secondary alteration, such as differences in Pr/n-C_{17} and Ts/Tm ratios. The tight clustering of samples in PCA score space, coupled with substantial overlap among oils from different depobelts, confirms that compositional differences are subtle and continuous rather than discrete. Importantly, no principal component clearly separates oils by depobelt or structural domain, reinforcing the interpretation that these oils belong to a genetically related population. Star plot comparisons corroborate this conclusion by demonstrating near-identical multi-parameter fingerprints for representative samples. Together, the statistical results indicate that observed geochemical variability is controlled primarily by minor maturity and migration effects rather than by fundamentally different source rocks or isolated charge systems.

Principal component analysis reduces multidimensional datasets into orthogonal axes representing the dominant sources of variance [25]. In this study, five components with eigenvalues ≥1 explain 79.48% of total variance, indicating that the dataset structure is well

captured by a limited number of controlling geological processes. PC1 accounts for 35.77% of total variance and is strongly influenced by Olea. Index, Olea./(Olea.+C_{30} Hop.), Pr/n-C_{17}, and Ster. Index. Oleanane is a well-established biomarker derived primarily from angiosperms and is characteristic of Tertiary deltaic systems influenced by higher-plant input [3]. Its strong loading confirms that terrestrial organic matter contribution is the dominant source of variability in the dataset.

The association of sterane-based indices with oleanane ratios further supports a higher-plant–dominated source facies. In deltaic petroleum systems, increased C_{29} sterane abundance relative to C_{27} steranes reflects significant land-derived organic input [27]. The prominence of PC1 therefore indicates that differences among oils are primarily controlled by variations in terrestrial organic matter contribution rather than fundamentally different depositional systems. The fact that PC1 represents the largest proportion of variance suggests that all oils share a broadly similar deltaic to paralic source facies, with only minor differences in organic matter proportions. PC2 explains 13.74% of the total variance and is dominated by strong loadings of Pr/Ph and Pr/(Pr+Ph), with a negative contribution from Ph/n-C_{18}. These ratios are widely used proxies for depositional redox conditions [35]. Higher Pr/Ph values typically indicate more oxic conditions, whereas lower values suggest suboxic to anoxic environments. The moderate variance explained by PC2 indicates that depositional redox conditions exert a secondary but significant control on oil composition. However, the PCA score distribution reveals substantial overlap among samples along PC2, implying that the range of redox conditions represented in the source rocks is relatively narrow. This limited dispersion suggests that the oils were generated from source intervals deposited under broadly similar redox regimes. PC3 accounts for 12.63% of total variance and is strongly influenced by Ts/(Ts+Tm), C_{29} 20S/(20S+20R), and CPI. These parameters are established maturity indicators reflecting isomerization equilibria and odd–even predominance reduction during thermal evolution [3],[18],[27].

The presence of a distinct maturity-related component indicates measurable but limited maturity variation among samples. However, because PC3 contributes substantially less variance than PC1, maturity differences are not the primary driver of compositional variability. Moreover, the PCA score plot shows no discrete clustering along the maturity axis, suggesting that maturity variations occur within a relatively narrow thermal window. PC4, dominated by Ster./Hop, likely reflects sterane–hopane balance variations that may result from subtle facies shifts or migration-related fractionation. PC5, influenced by C_{29}/C27 sterane ratios and C_{32} hopane isomerization, captures minor differences in organic input proportions and equilibrium maturity states. Together, PC4 and PC5 explain less than 18% of the total variance, indicating that these effects are subordinate. Their relatively minor contribution reinforces the overall compositional homogeneity of the oil population.

The correlation matrix reveals strong positive associations among redox-sensitive and terrestrial input proxies. For example, the high correlation between Pr/Ph and Pr/(Pr+Ph) confirms redundancy in redox indicators, while the near-perfect association between Olea. Index and Olea./(Olea. +C30 Hop.) confirms strong coherence among angiosperm-derived biomarkers. Such redundancy explains why these variables cluster strongly within PC1 and PC2. In multivariate datasets, highly correlated variables amplify the influence of shared geological controls [25]. The dominance of these correlated biomarker groups underscores the importance of terrestrial input and depositional conditions in defining oil composition.

The radar plots (Figure 14 and Figure 15) provide a graphical representation of relative biomarker distributions. The near-overlapping polygon geometries among samples indicate that the relative proportions of diagnostic biomarkers remain consistent across depobelts. In petroleum fingerprinting, visually similar radar profiles suggest shared source characteristics and similar generation histories [3],[9],[16]. The limited deviation along individual axes such as Ts/(Ts+Tm) or CPI is consistent with minor maturity variation but does not alter the overall fingerprint architecture. The visual coherence of the radar diagrams corroborates the statistical findings from HCA and PCA, reinforcing the interpretation of genetic uniformity.

Implications for Reservoir Connectivity and Charge System Continuity

The strong geochemical similarity observed across structurally and geographically distinct reservoirs has important implications for reservoir connectivity in the Niger Delta Basin. The clustering of oils from different depobelts into a single dominant oil family suggests basin-scale charge continuity and extensive lateral and vertical migration of hydrocarbons [8],[9]. This interpretation is consistent with the structural framework of the basin, in which growth faults and shale mobility provide both vertical migration pathways and opportunities for cross-fault leakage during active deformation [5],[10],[36],[37]. It is important to distinguish between geochemical connectivity and dynamic connectivity. While geochemical similarity indicates that reservoirs were charged by the same petroleum system and likely experienced interconnected migration pathways during geological time, it does not necessarily imply present-day pressure communication or production-scale connectivity. Fault sealing, shale smear development, and post-charge deformation may isolate reservoirs dynamically even when their oils are genetically identical. An alternative explanation for the observed similarity is extensive oil mixing during migration rather than direct reservoir-to-reservoir communication. However, the consistency of biomarker ratios across multiple independent parameters, combined with the lack of distinct sub-families in both HCA and PCA, suggests that mixing occurred within a broadly unified charge system rather than through random pooling of unrelated oils. This supports a model in which hydrocarbons generated from compositionally similar source rocks were redistributed across the basin through shared migration networks.

The multivariate statistical coherence has significant implications for reservoir continuity. If compartmentalization or multiple independent charge systems were present, one would expect distinct clusters in both dendrogram and PCA score space [2],[4]. Instead, the consistent overlap and low linkage separation indicate that hydrocarbons across structural provinces share a common origin and migration history [38],[39],[40]. Such compositional homogeneity suggests effective lateral migration pathways and regional charge distribution. The absence of discrete oil families implies that structural segmentation has not resulted in isolated petroleum systems. Rather, the data supports a unified petroleum system with broad areal extent and strong connectivity. From a production and reservoir management perspective, this genetic uniformity implies that fluid properties are likely to be comparable across fields, facilitating correlation and field-wide development strategies. The integrated statistical evidence therefore supports the interpretation that the investigated crude oils are genetically homogeneous and derived from a common source facies within a unified petroleum system exhibiting strong reservoir continuity.

CONCLUSIONS

This study applied integrated oil geochemical fingerprinting and multivariate statistical analysis to evaluate reservoir connectivity across major depobelts of the Niger Delta Basin. Whole-oil gas chromatography and biomarker data reveal a high degree of compositional similarity among crude oils from structurally and geographically distinct reservoirs, indicating derivation from compositionally similar source rocks deposited under deltaic to shallow-marine conditions and generated within a comparable thermal maturity window. Hierarchical cluster analysis and principal component analysis consistently group the oils into a single dominant genetic family, with only minor internal variability related to subtle maturity or migration effects. The lack of systematic separation by depobelt or structural domain demonstrates that present-day structural compartmentalization does not necessarily reflect geochemical isolation. Instead, the results point to basin-scale charge continuity and extensive lateral and vertical hydrocarbon migration within the Niger Delta petroleum system.

These findings highlight the distinction between geochemical connectivity and dynamic reservoir communication and underscore the value of oil geochemistry as a time-integrated tool for connectivity assessment. Incorporating geochemical and statistical methods alongside structural and dynamic data can significantly reduce uncertainty in reservoir management, field redevelopment, and exploration risk assessment in structurally complex deltaic basins.

REFERENCES

[1] Kaufman, R.L., Ahmed, A.S., Elsinger, R.J., Gas Chromatography as a development and production tool for fingerprinting oils from individual reservoirs: applications in the Gulf of Mexico. In: Schumaker, D., Perkins, B.F. (eds.) Proceedings of the 9th Annual Research Conference of the Society of Economic Paleontologists and Mineralogists New Orleans, pp. 263–282. 1990.

[2] Kaufman, R., L., Dashti, H., Kabir, C.S., Pederson, J.M., Moon, M.S., Quttainah, R., Al Wael, H., Characterizing the Greater Burgan field: use of geochemistry and oil fingerprinting. SPE Reserv. Eval. Eng., v. 5 (3), pp. 190–196. 2002.

[3] Peters, K.E, Walters, C.C., Moldowan, J.M., The Biomarker Guide: Biomarkers and isotopes in petroleum systems and Earth history (Vol. 2), 2nd edition, Cambridge University Press, New York. 2005.

[4] Anyanwu, T.C., Ekpo B.O., Petroleum system, filling history and age appraisal of source rocks of the Niger Delta Basin: Fingerprinting of pentacyclic triterpenoids. Energy Geoscience, 6:100399. 2025.

[5] Evamy, B.D., Haremboure, J., Kamerling, P., Knaap, W.A., Molloy, F.A., Rowlands, P.H., Hydrocarbon habitat of Tertiary Niger Delta. AAPG Bull., v. 62, pp. 277-298. 1978.

[6] Doust, H., Omatsola, E., Niger Delta. In: J.D., Edwards, P.A. Santogrossi, (eds.). Divergent/passive Margin Basins, AAPG Memoir, 48, pp. 239–248. 1990.

[7] Ukpong, A.J., Anyanwu, T.C., Osung W.E. Omoko, E.N., Sequence Stratigraphic Study of B-24 Well‖ Northern Depobelt, Niger Delta, Southeastern Nigeria. Journal of Applied Geology and Geophysics, 6 (2), 20-28. 2018.

[8] Abrakasa, S., Muhammad, A.B., Infilling Direction and Fluid Communication in the E2.0 Reservoir of the Kolo Creek Oil Field, Niger Delta Nigerian Journal of Basic and Applied Science, 16(2), 115-121, 2008.

[9] Ekpo, B.O., Essien, N., Neji, P.A. Etsenake, R.O., Geochemical fingerprinting of western offshore Niger Delta oils. Journal of Petroleum Science and Eng., 160, 452–464, 2018.

[10] Corredor, F., Shaw, J. H., Bilotti, F., Structural styles in the deep-water fold and thrust belts of the Niger Delta. AAPG Bull., 89(6), 753–780. 2005.

[11] Peters, K.E., Moldowan, J.M., The Biomarker Guide: Interpreting Molecular Fossils in Petroleum and Ancient Sediments. Prentice Hall, Englewood Cliffs, New Jersey, pp. 211. 1993.

[12] Hwang, R.J., Ahmed, A.S., Moldowan, J.M., Oil composition variation and reservoir continuity: Unity Field, Sudan. Organic Geochemistry, 21, 171–188. 1994.

[13] Bustin, R.M., Sedimentology and characteristics of dispersed organic matter in Tertiary Niger Delta: origin of source rocks in a deltaic environment. AAPG Bull., 72, 277-298. 1988.

[14] Haack, R.C., Sundararaman, P., Diedjomahor, J.O., Xiao, H., Gant, N.J., May, E.D., Kelsch, K., Niger Delta petroleum systems, Nigeria. In: M.R. Mello and B.J., Katz, (eds.) Petroleum systems of South Atlantic margins. AAPG Memoir, pp. 213–231. 2000.

[15] Sonibare, O., Alimi, H., Jarvie, D., Ehinola, O.A., Origin and occurrence of crude oil in the Niger delta, Nigeria. Journal of Petroleum Science and Eng., 61, 99–107. 2008.

[16] Anyanwu, T.C, Ekpo, B.O., Oriji, B.A., Geochemical Characterization of the Coastal and Offshore Niger Delta Crude Oils, Nigeria, International Journal of Advanced Academic Research, 7 (12), 73-87. 2021.

[17] Egbo, O.K., Adeigbe, O.C., Esegbue O., Biomarker Fingerprinting of crude oils from Niger Delta depobelts, Nigeria. Journal of African Earth Sciences, 231, 105768, 2025.

[18] Anyanwu, T.C, Ekpo, B.O., Oriji, B.A., Biomarker application in the recognition of the geochemical characteristics of crude oils from the five depobelts of the Niger Delta basin, Nigeria, Iranian Journal of Earth Sciences, 14 (1), 1-17. 2022.

[19] Onyekuru, S.O., Achukwu-Ononye O.U., Ukpong A.J., Ofoh I.J., Ibeneme S.I., Anyanwu T.C., Stratigraphy and Paleoenvironment(s) of the Late Cretaceous Deposits in Ohafia Area, Afikpo Basin, Southeastern Nigeria. Journal of African Earth Sciences, 197, 104713. 2023.

[20] Onyekuru, S.O., Adumekwe, O. V., Ukpong, A.J., Ikoro, D.O., Anyanwu, T.C, Ofoh, I.J., Sequence stratigraphic interpretation of Middle–Late Miocene successions of OMAH–1 well Offshore Niger Delta, Nigeria. Iranian Journal of Earth Science (IJES), 17(2), 1-14, 2025.

[21] Ukpong, A.J., Anyanwu, T.C., Late Eocene—Early Oligocene Foraminiferal Biostratigraphy and Paleoenvironment of Sediments from "Beta- 24 Well" Niger Delta Basin, South Eastern Nigeria. European Academic Res., 6(2), 871-891, 2018.

[22] Nwaejije, E.C., Obiosio, E.O., Hamidu, Foraminifera Biostratigraphy and Paleoenvironment of Well 5, OML 34, Niger Delta, Nigeria. Palaeontologia Electronica. 20.3.51A: 1-17, 2017.

[23] Ukpong A.J., Ekhalialu O. M., Sequence Stratigraphic Analysis of Siliciclastic Sediments from the Agbada Formation in the Niger Delta: A Well Log – Foraminifera Approach. Journal of Mining and Geology, 57 (2): 299–314. 2021.

[24] Owono, F.M., Atangana, J.N., Owona, S., Dauteuil, O., Ngapna, M.N., Guillocheau, F., Koum, S., Boum, R.B.E., Ntamak-Nida, M.J., Tectono-stratigraphic evolution and architecture of the Miocene Rio del Rey basin (Cameroon margin, Gulf of Guinea). International Journal of Earth Sciences. Springer. 2020.

[25] Jolliffe, I.T., Cadima, J., Principal component analysis: A review and recent developments. Philosophical Transactions of the Royal Society A, 374(2065), 20150202. 2016.

[26] El-Sheshtawy, H.S., Khalil, N., Farouk, S., Biodegradation Effect on the Campanian Oil Shale of Egypt, Geomicrobiology Journal, 37(8): 746-752. 2020.

[27] Tissot, B.P., Welte, D.H., Petroleum Formation and Occurrence. Springer-Verlag, New York. 1984.

[28] Pampanin, D.M., Sydens, M.O., Presence and influence in the aquatic environment. In Polycyclic aromatic hydrocarbons a constituent of petroleum. Intech, pp. 83-118. 2013.

[29] Bray, E.E., Evans, E.D., Distribution of n-paraffins as a clue to recognition of source beds. Geochimica et Cosmochimica Acta, 22, 2-15. 1961.

[30] Mackenzie, A.S., Lamb, N.A., Maxwell, J.R., Steroid hydrocarbons and the thermal history of sediments. Nature, 295, 223–226. 1982.

[31] Dahi, J., Moldowan, J.M., Sundararaman, P., Relationship of biomarker distribution to depositional environment: Phosphoria Formation, Montana, U.S.A, Organic Geochemistry, 20 (7):1001–1017. 1999.

[32] El-Sabagh, S. M., Ebiad, M. A., Rashad, A. M., El-Naggar, A. Y., Badr, I.H.A., El Nady, M.M., Abdullah, E.S., Characterization Based on Biomarkers Distribution of Some Crude Oils in Gulf of Suez Area – Egypt. Journal of Materials and Environmental Sciences, 8:1-15. 2017.

[33] Anyanwu, T.C., Agbi, I.O., Takyi, B., Njoku, J.O., Ugbaja, U.A., Biological Marker Fingerprints of Crude Oils from Three Oilfields in the Central Niger Delta: Implication to Source Input, Conditions of Deposition, and Thermal Maturation. GeoScience Engineering, 68 (2), 134–150. 2022.

[34] El Diasty, W.S., Moldowan J.M., Application of biological markers in the recognition of the geochemical characteristics of some crude oils from Abu Gharadig Basin, north Western Desert Egypt. Marine and Petroleum Geology, 35:28-40. 2012.

[35] Hunt, J.M., Petroleum Geochemistry and Geology, 2nd Edition, W.H. Freeman and Company, U.S.A., 1996.

[36] Adegoke, O.S., Oyebamiji, A.S., Edet, J.J., Osterloff, P.L., Ulu, O.K., Cenozoic Foraminifera and Calcareous Nannofossil Biostratigraphy of the Niger Delta. Elsevier, Radarweg 29, PO Box 211, 1000 AE Amsterdam, Netherlands, 2017.

[37] Saugy, I., Eyer, J.A., Fifty years of exploration in the Niger Delta (West Africa). In: Halbouty M.T. (ed) Giant oil and gas fields of the decade1990–1999, vol 78. AAPG Memoir, Tulsa, pp 221–226, 2003.

[38] Samuel, O.J., Cornford, C., Jones, M., Adekeye, O.A., Akande, S.O., Improved understanding of the petroleum systems of the Niger Delta Basin, Nigeria. Organic Geochemistry, 40, 461-483. 2009.

[39] Fang, R., Li, M., Lu, H., Wang, T.G., Yuan, Y., Liu, Y., Ni, Z., Oil charging history and pathways of the Ordovician carbonate reservoir in the Tuoputai region, Tarim Basin, NW China. Petroleum Science, 14, 662-675. 2017.

[40] Seifert, W.K., Moldowan, J.M., The effect of thermal stress on source-rock quality as measured by hopane stereochemistry. Physics and Chemistry of the Earth, v. 12, pp. 229-237. 1981.

Received: March 2026; Revised: May 2026; Accepted: May 2026; Published: May 2026